Electronic Supplementary Information

for the manuscript entitled

Selective sensing of ATP by hydroxide-bridged dizinc(II) complexes offering hydrogen bonding cavity

Deepak Bansal and Rajeev Gupta*

Department of Chemistry, University of Delhi, Delhi – 110 007 (India)

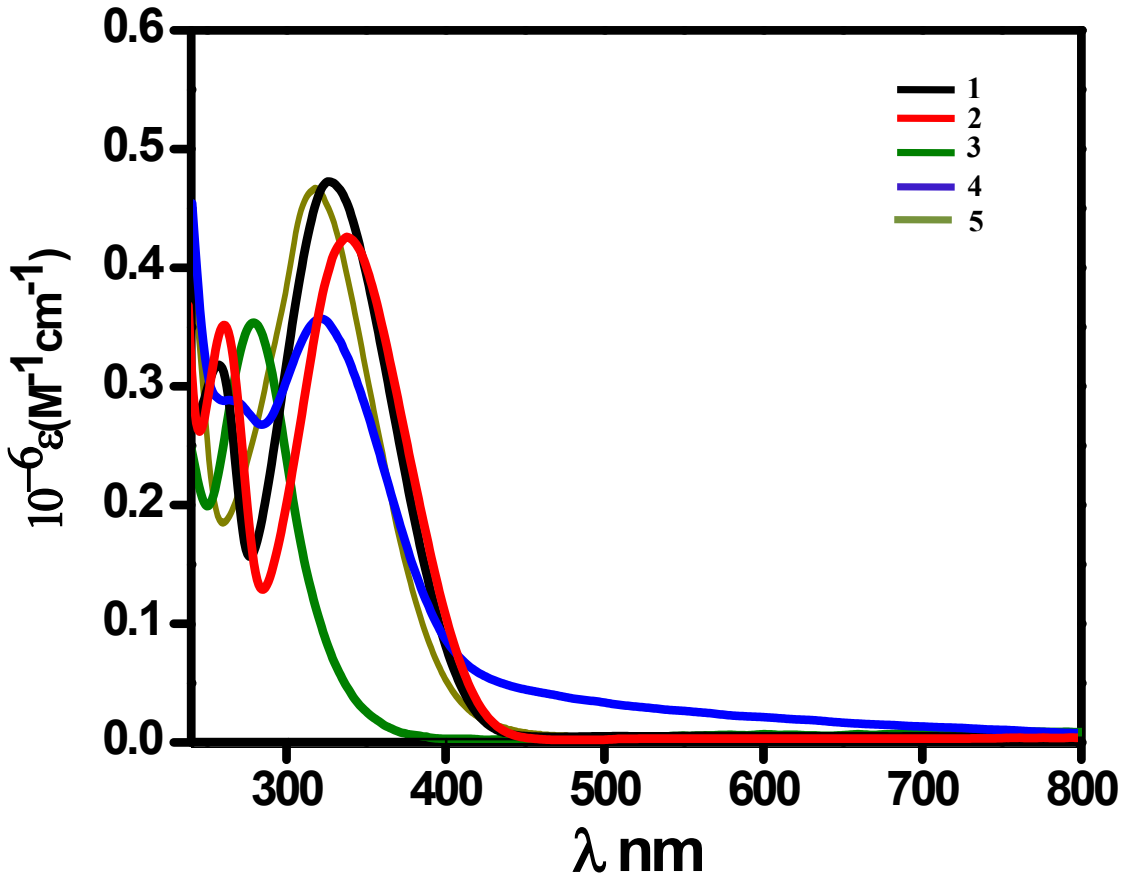

Figure S1. Absorption spectra of dizinc(II) complexes **1-5** measured in DMF.

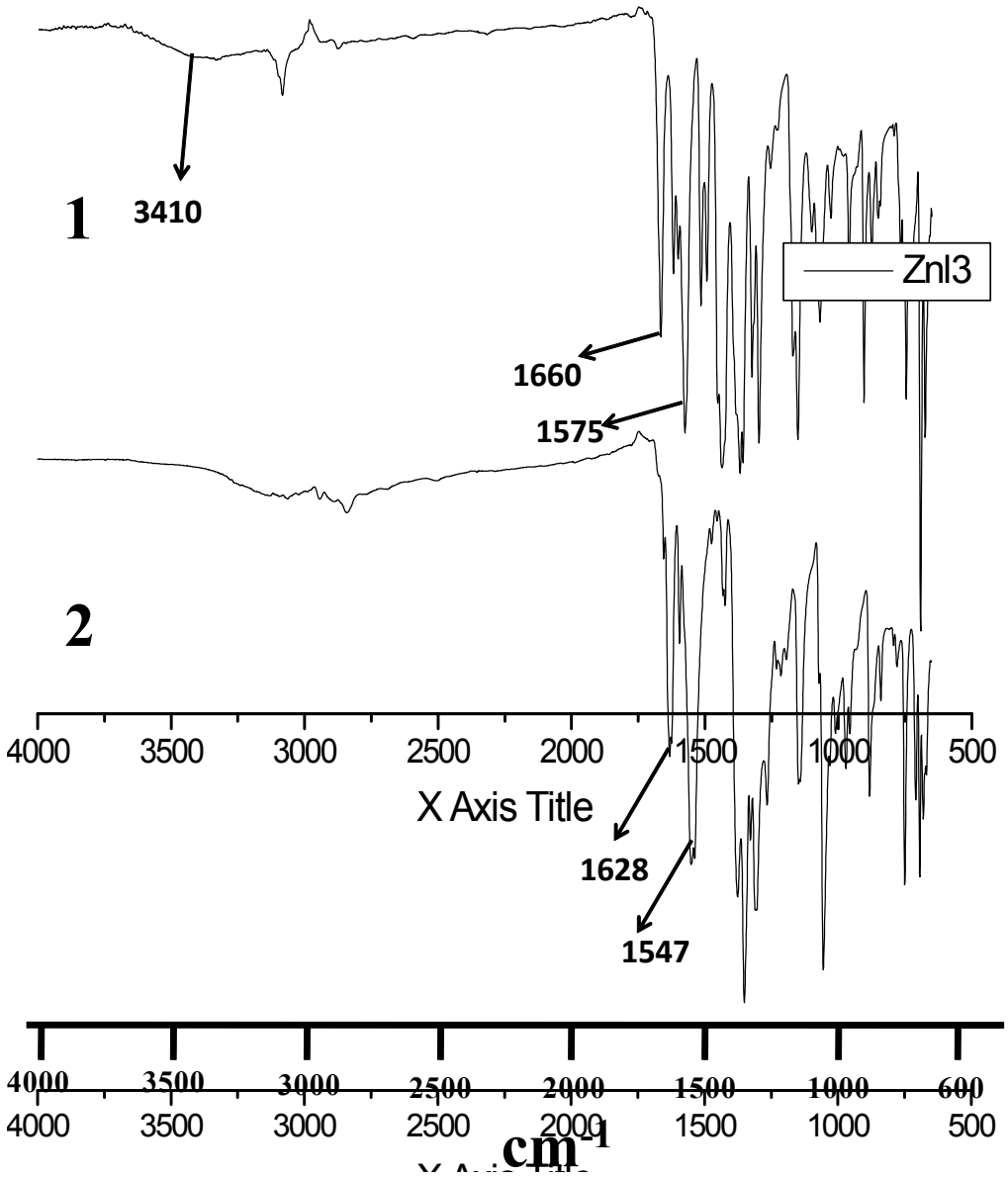

Figure S2. FTIR spectra of complexes **1** and **2**.

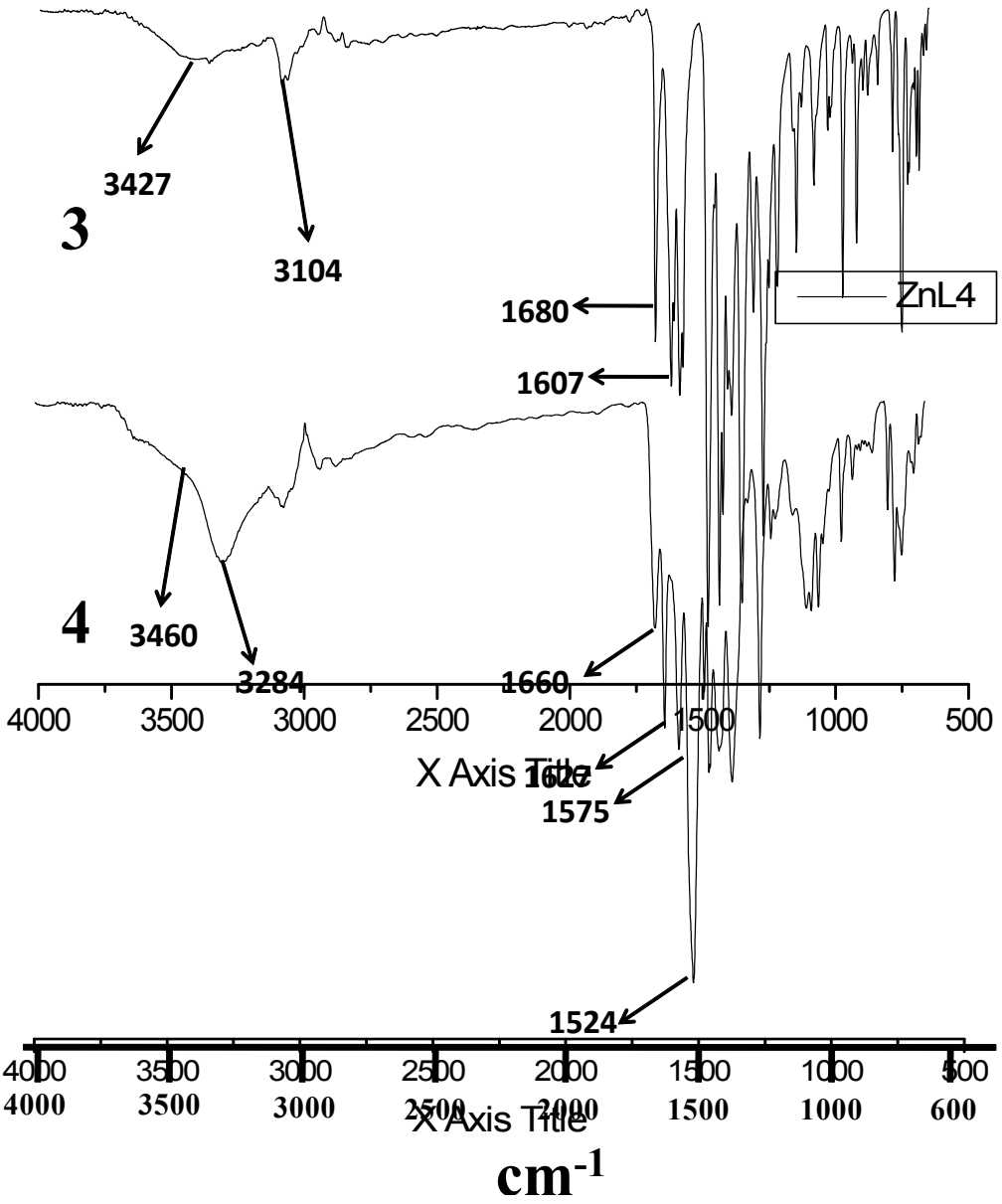

Figure S3. FTIR spectra of complexes **3** and **4**.

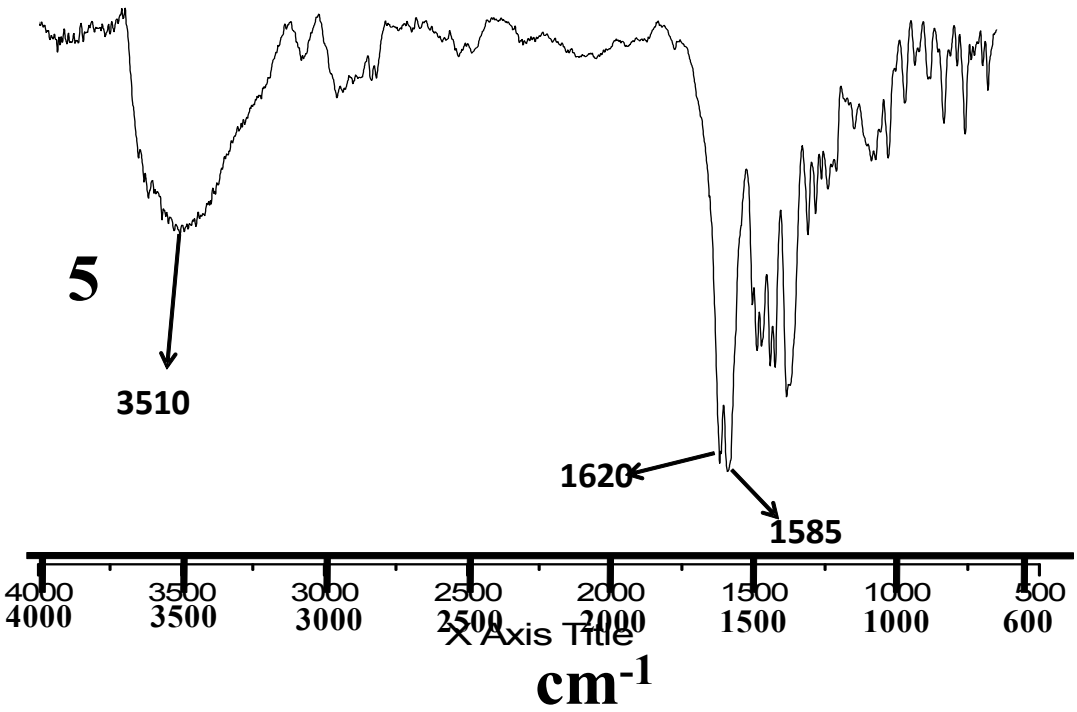

Figure S4. FTIR spectrum of complex **5**.

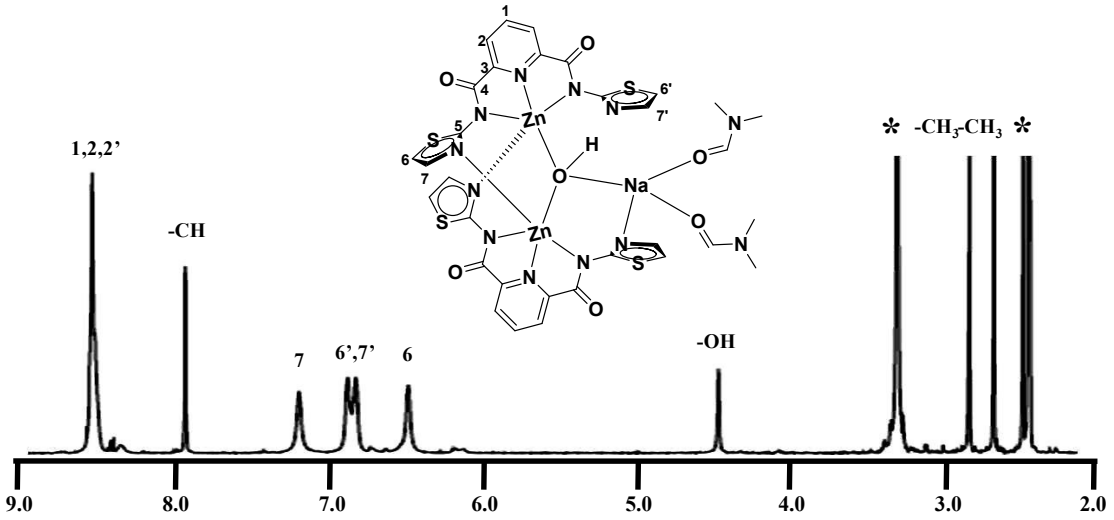

Figure S5. ^{1}H NMR spectrum of complex **1** in d_6-DMSO. *represents the residual solvent and/or adventitious H_2O peaks.

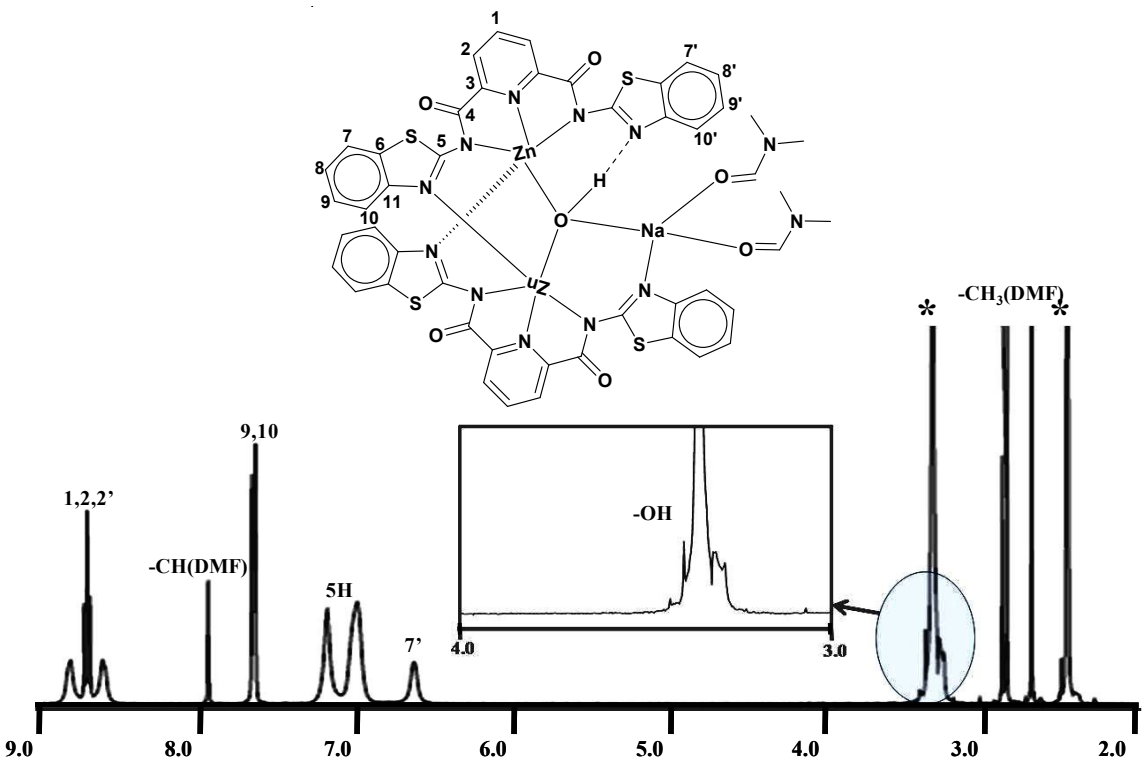

Figure S6. ^{1}H NMR spectrum of complex **2** in d_6-DMSO. *represents the residual solvent and/or adventitious H_2O peaks.

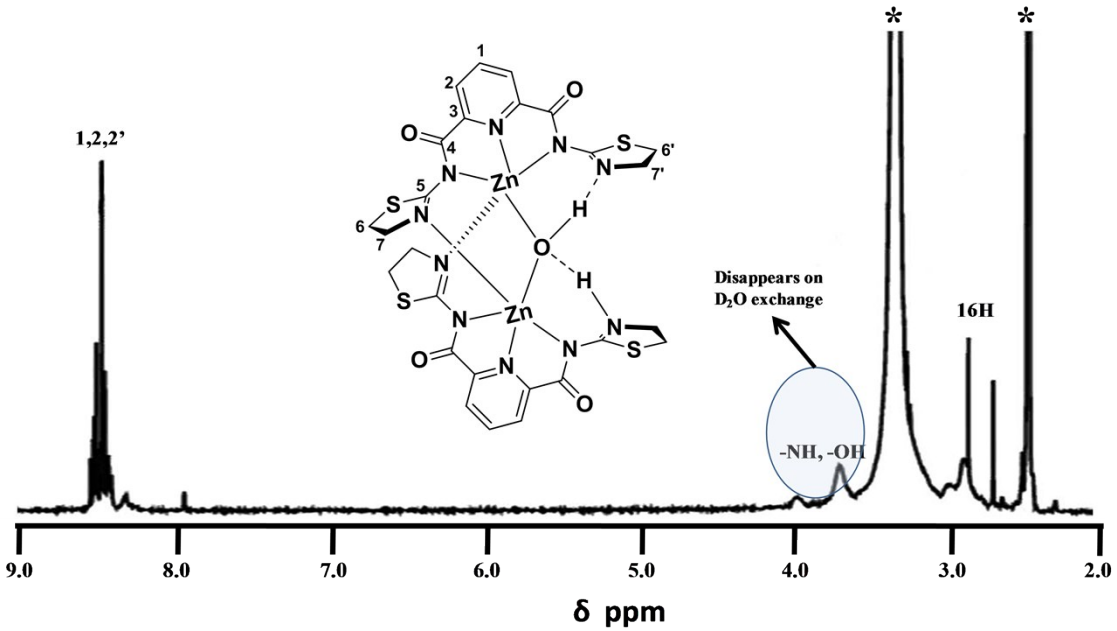

Figure S7. ^{1}H NMR spectrum of complex **3** in d_6-DMSO. *represents the residual solvent and/or adventitious H_2O peaks.

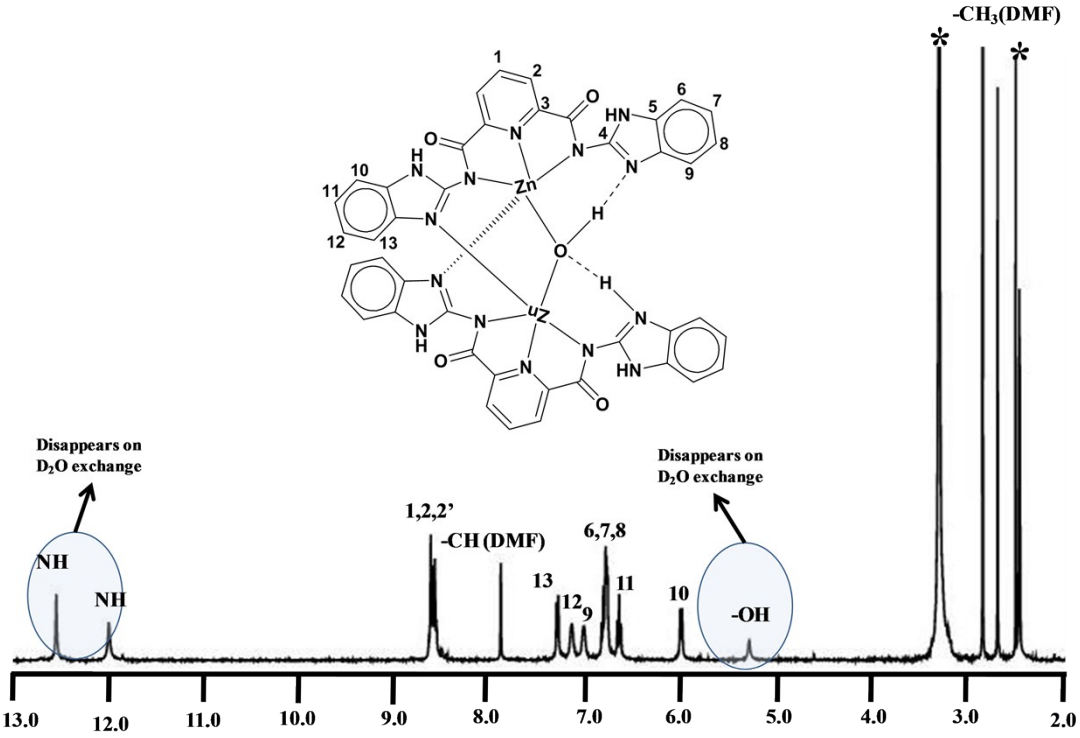

Figure S8. ^{1}H NMR spectrum of complex **4** in d_6-DMSO. *represents the residual solvent and/or adventitious H_2O peaks.

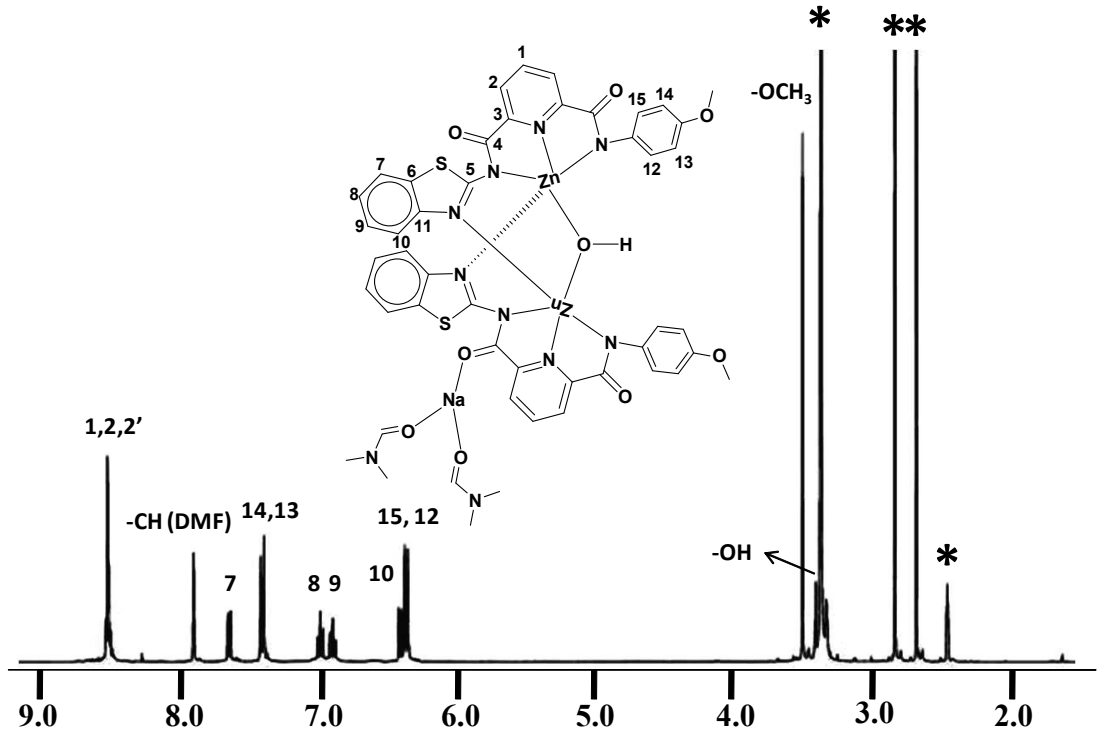

Figure S9. ^{1}H NMR spectrum of complex **5** in d_6-DMSO. *represents the residual solvent and/or adventitious H_2O peaks.

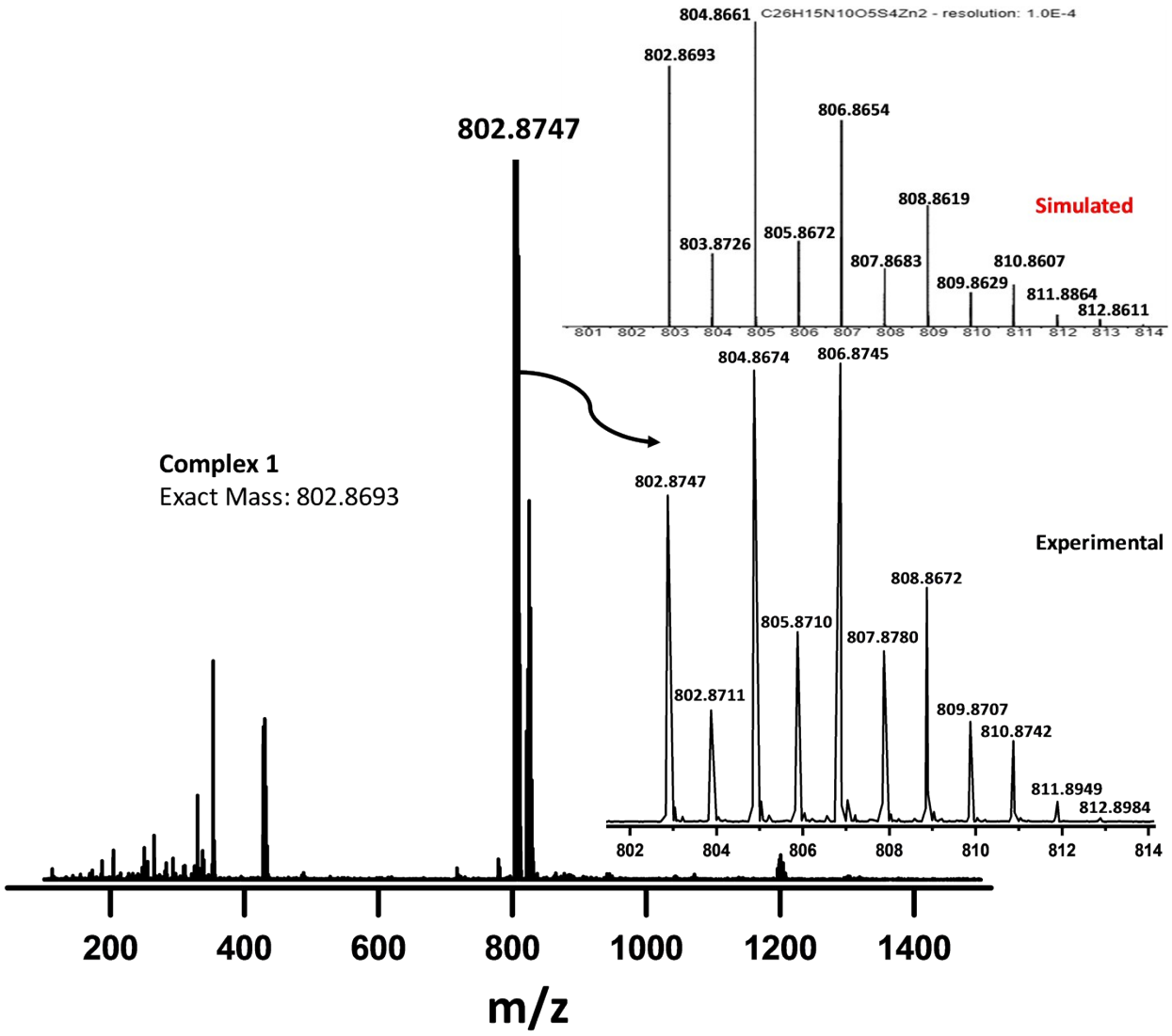

Figure S10. High resolution mass spectrum of complex **1** recorded in negative mode in DMF.

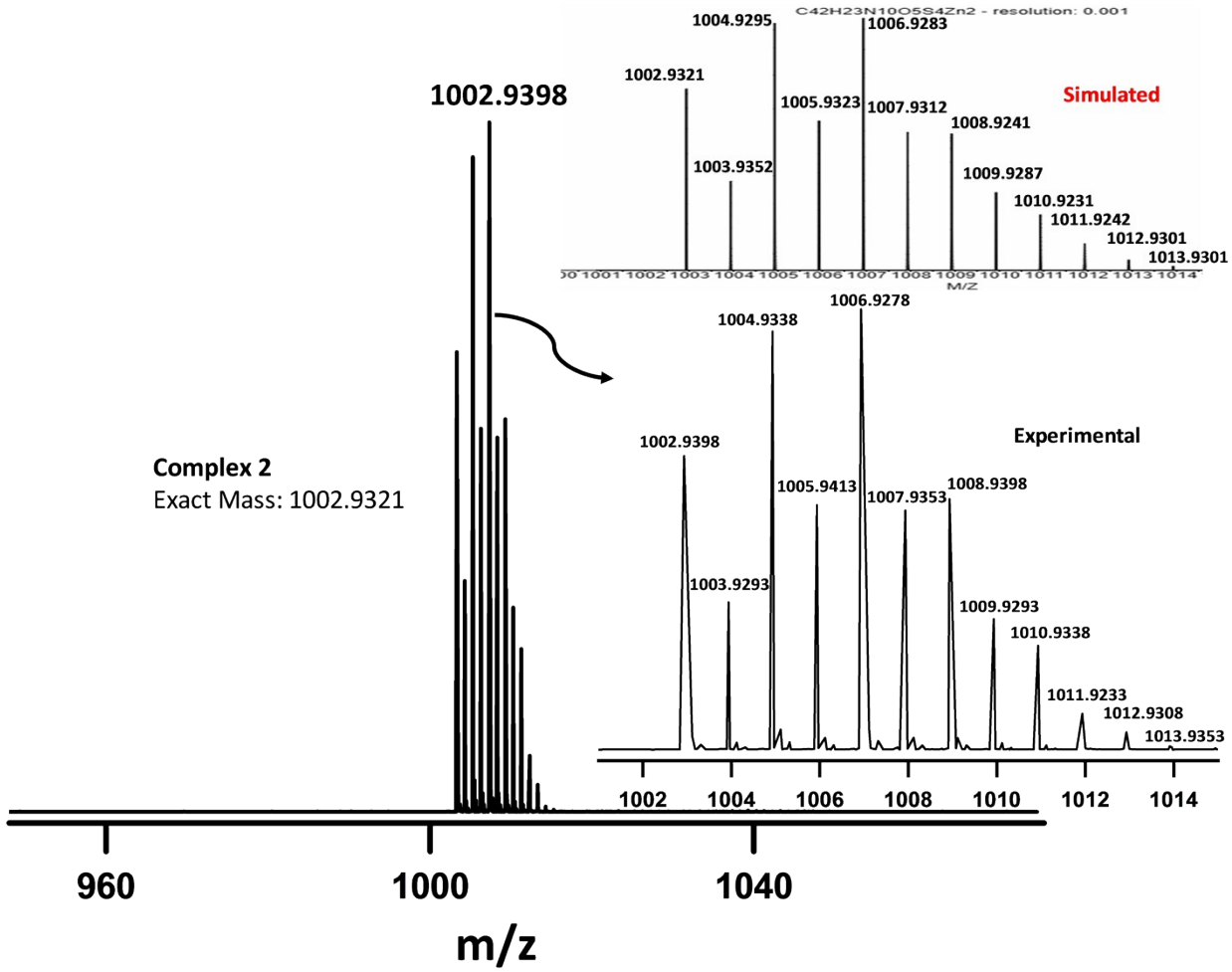

Figure S11. High resolution mass spectrum of complex **2** recorded in negative mode in DMF.

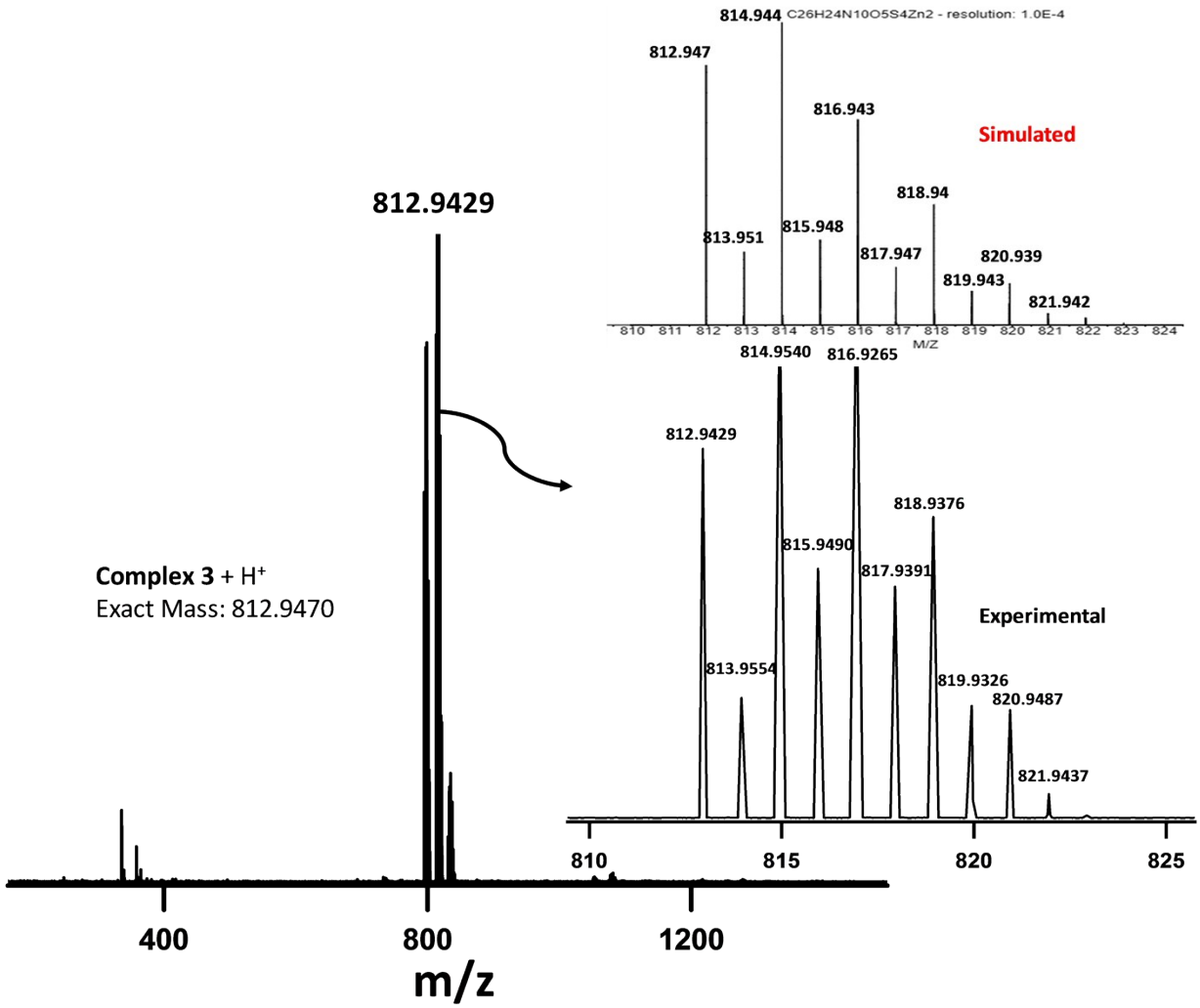

Figure S12. High resolution mass spectrum of complex **3** recorded in positive mode in DMF.

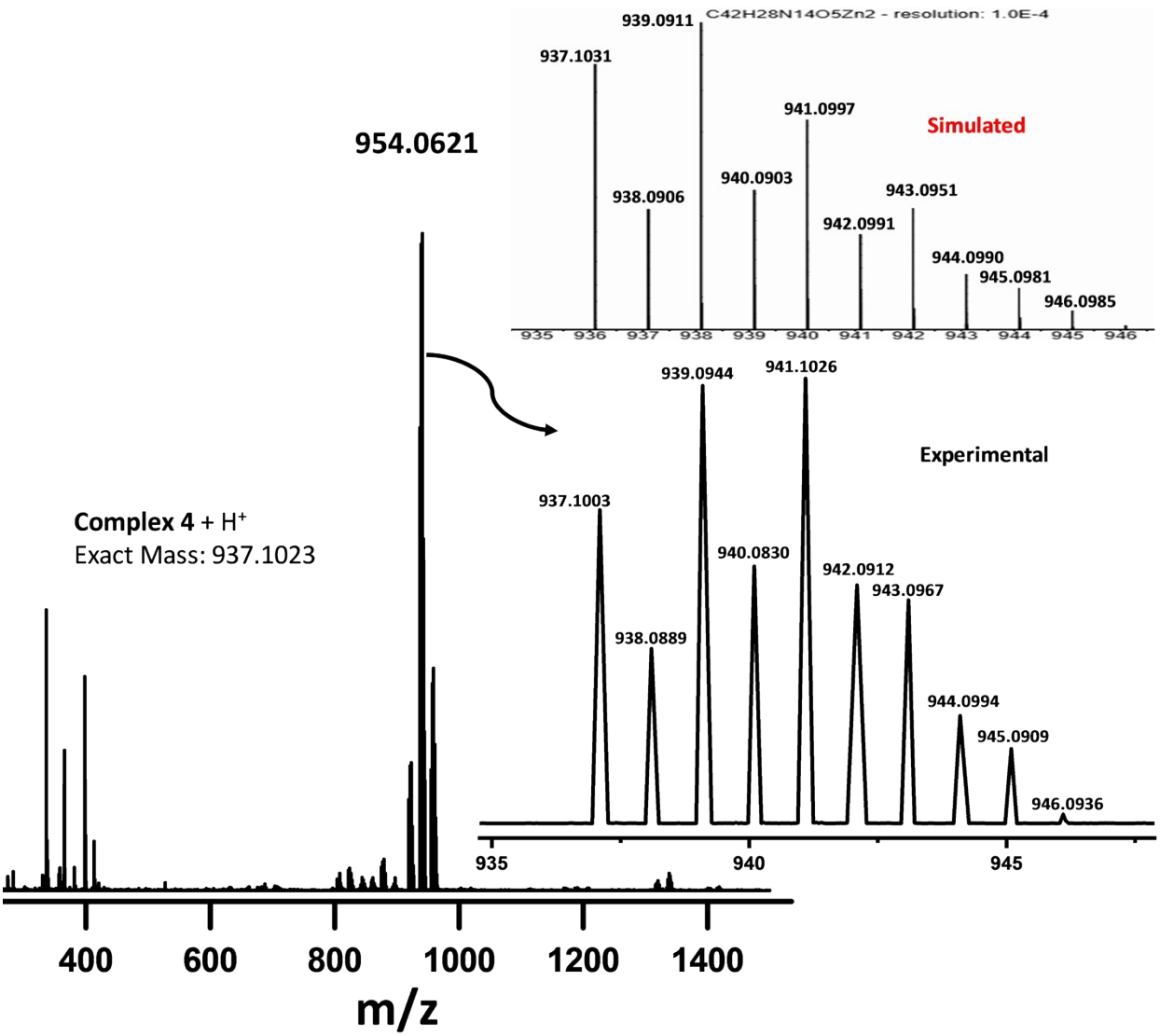

Figure S13. High resolution mass spectrum of complex **4** recorded in positive mode in DMF.

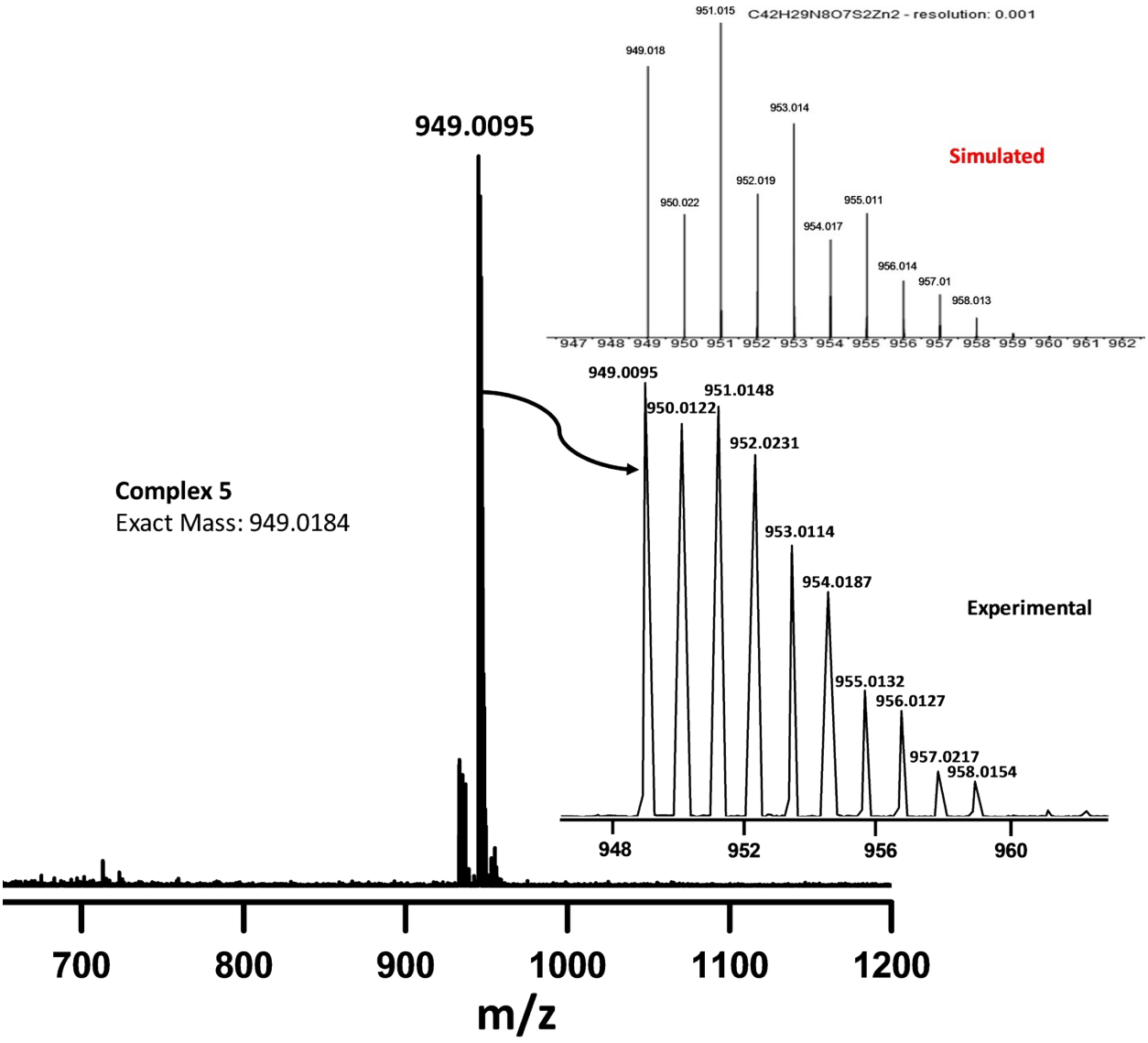

Figure S14. High resolution mass spectrum of complex **5** recorded in negative mode in DMF.

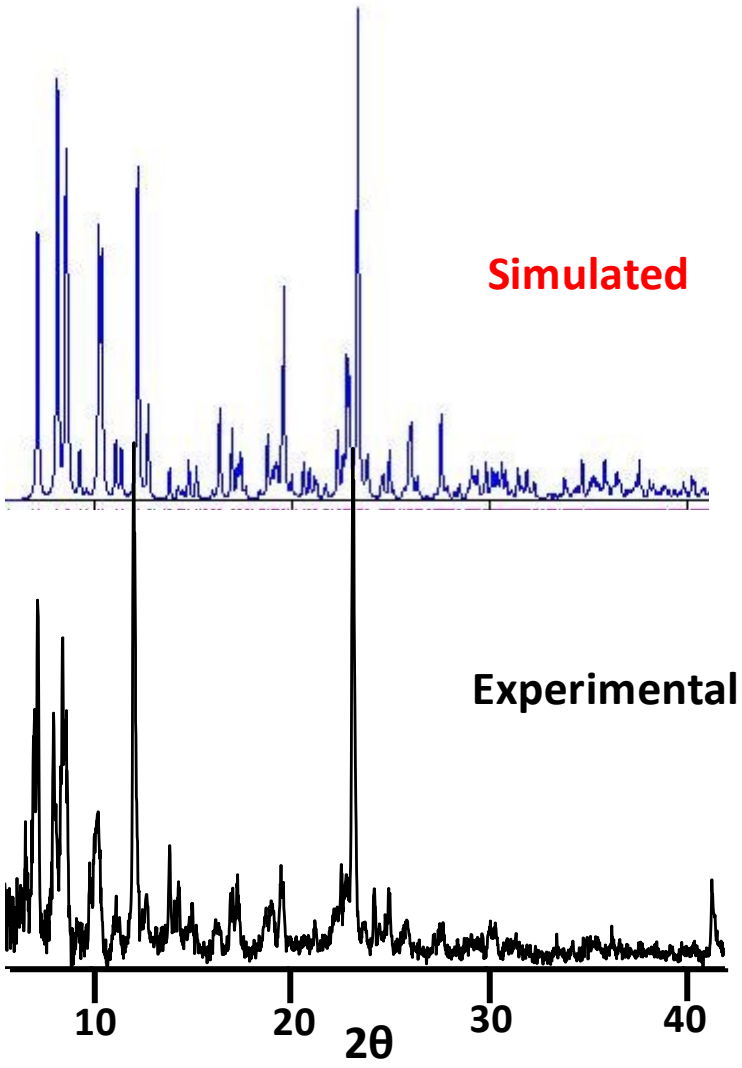

Figure S15. Powder XRD pattern for the bulk sample of complex **1** (black trace) and its comparison with the simulated pattern generated from the single crystal diffraction data using mercury version 3.6 (blue trace).

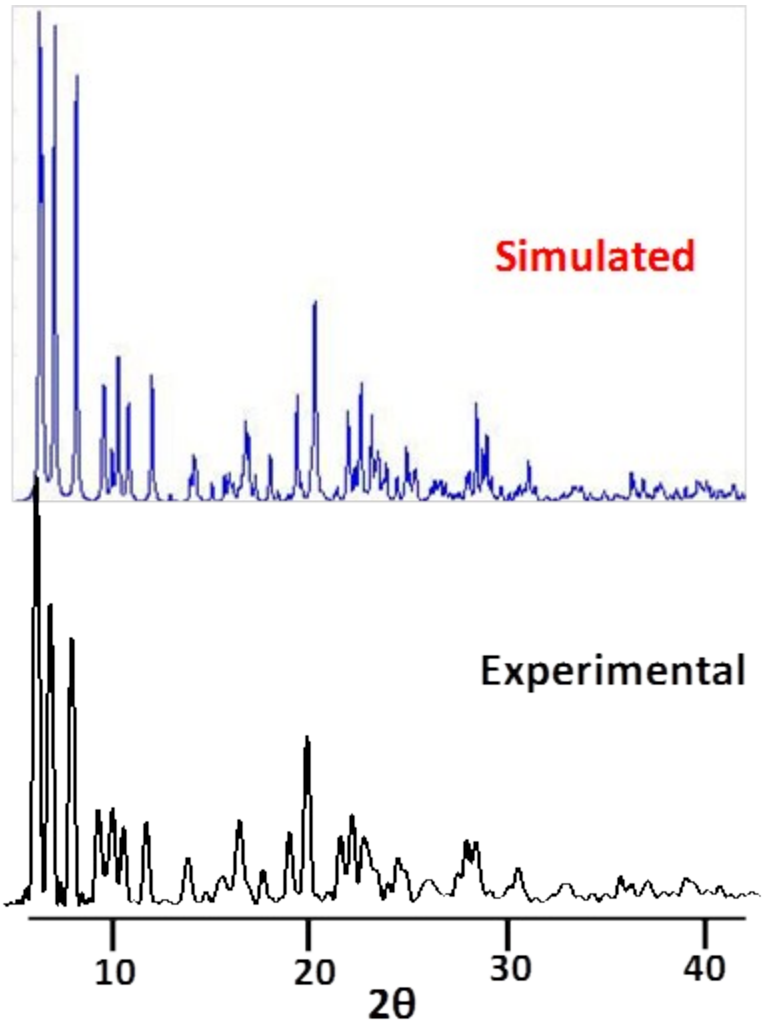

Figure S16. Powder XRD pattern for the bulk sample of complex **2** (black trace) and its comparison with the simulated pattern generated from the single crystal diffraction data using mercury version 3.6 (blue trace).

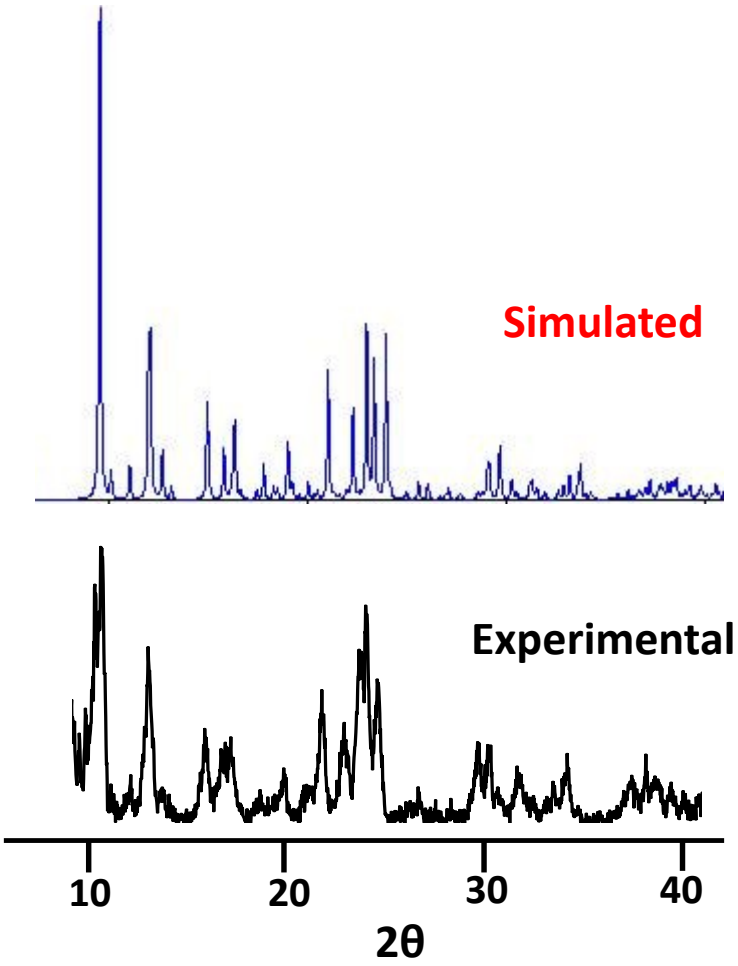

Figure S17. Powder XRD pattern for the bulk sample of complex **3** (black trace) and its comparison with the simulated pattern generated from the single crystal diffraction data using mercury version 3.6 (blue trace).

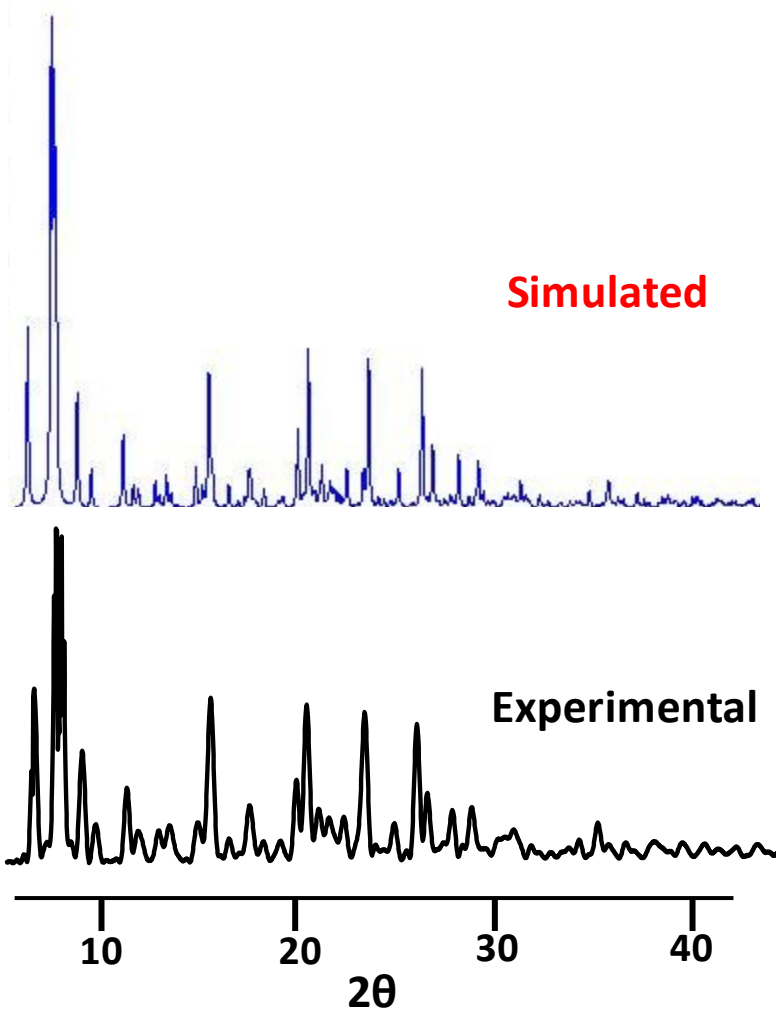

Figure S18. Powder XRD pattern for the bulk sample of complex **4** (black trace) and its comparison with the simulated pattern generated from the single crystal diffraction data using mercury version 3.6 (blue trace).

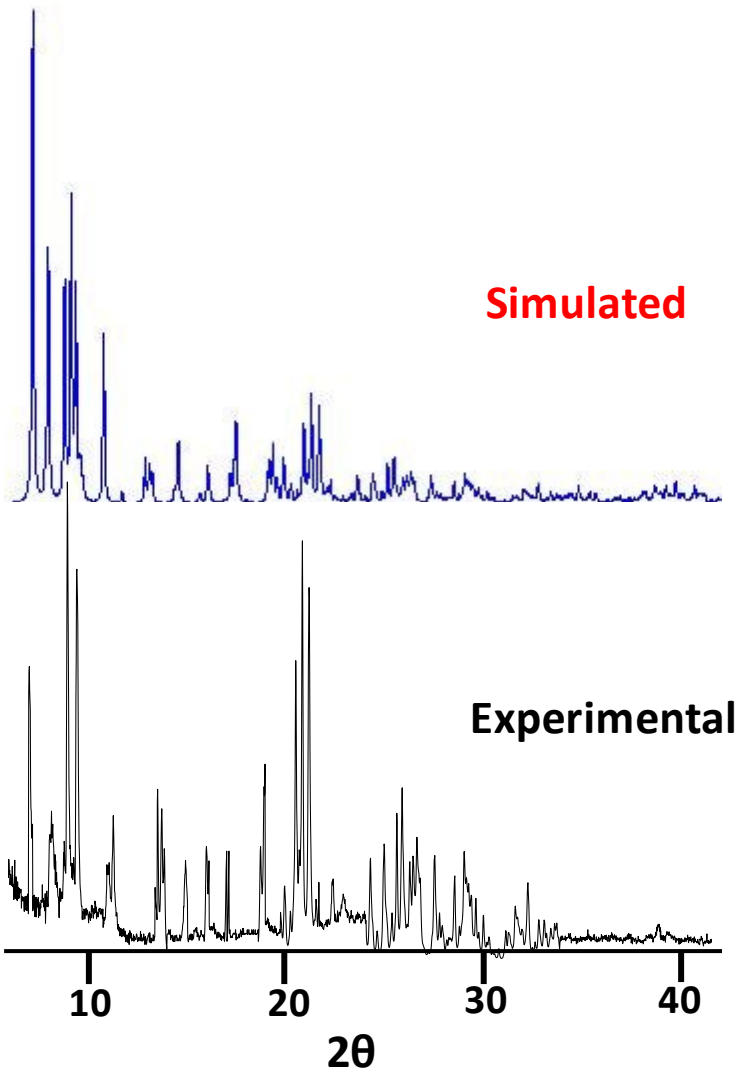

Figure S19. Powder XRD pattern for the bulk sample of complex **5** (black trace) and its comparison with the simulated pattern generated from the single crystal diffraction data using mercury version 3.6 (blue trace).

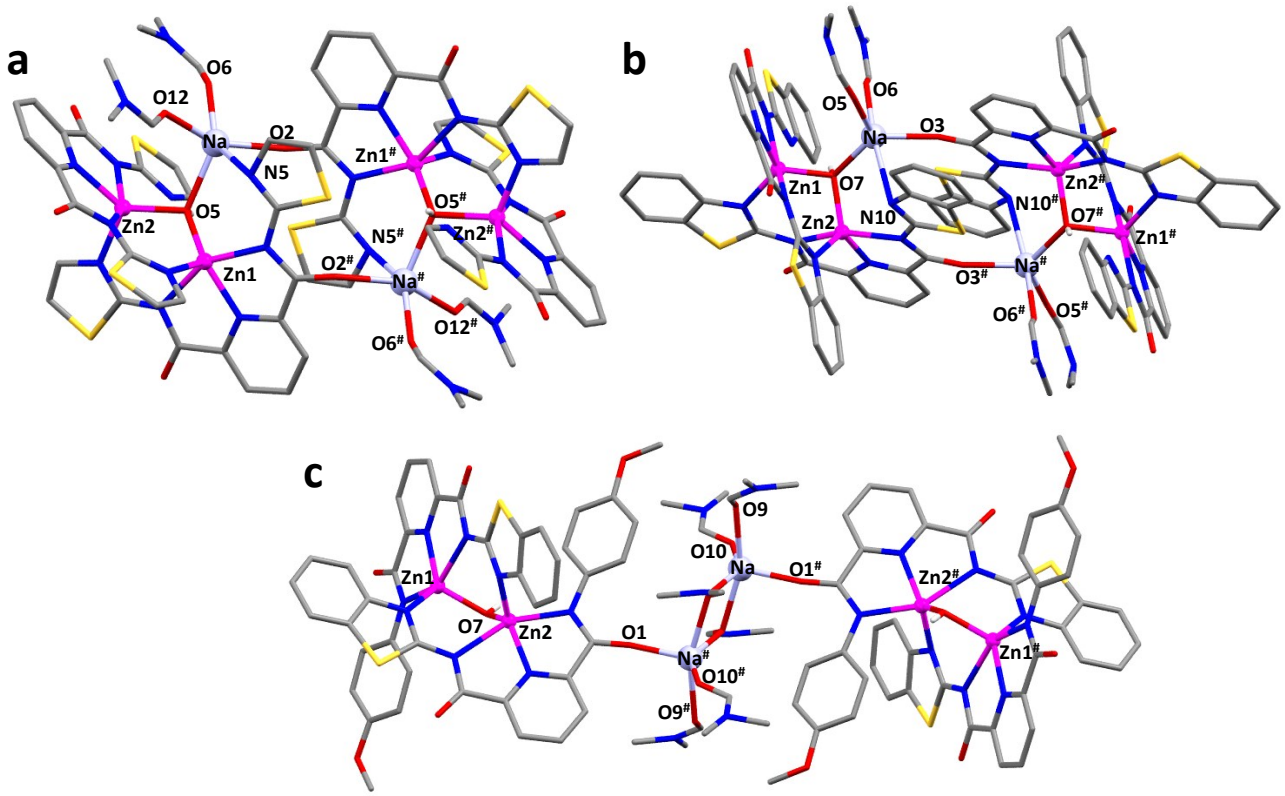

Figure S20. Capped and stick representation of dimer of dimers form for dizinc(II) complexes **1** (a), **2**(b) and **5**(c). In all cases Na^+ ions connect two Zn-based dimers together.

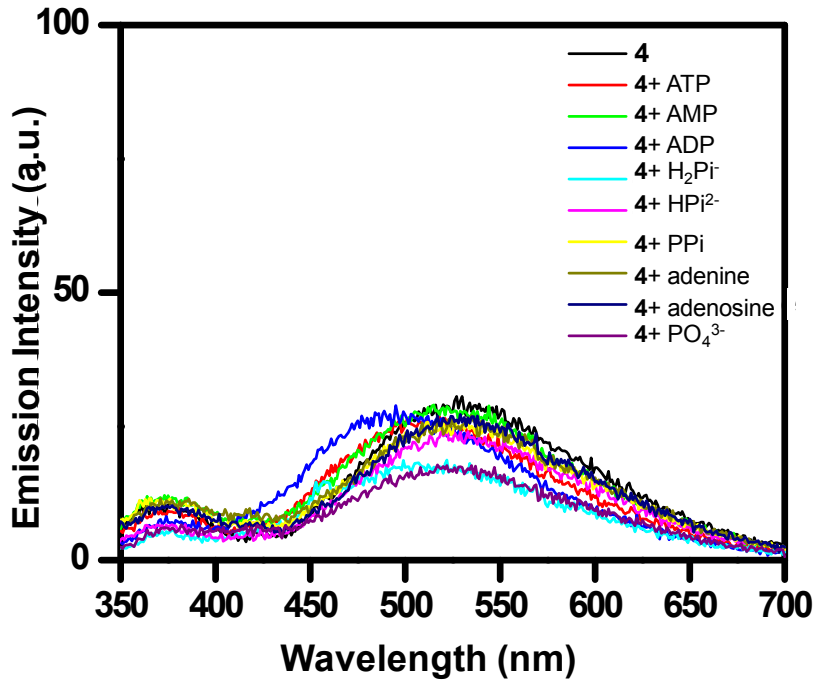

Figure S21. Emission spectra for complex **4** (50 μM) exhibiting negligible change in the emission intensity upon addition of different phosphate ions (5 equiv.). Conditions: solvent; DMSO-H_2O 10% v/v, HEPES, 7.2 pH, λ_{ex} = 330 nm.

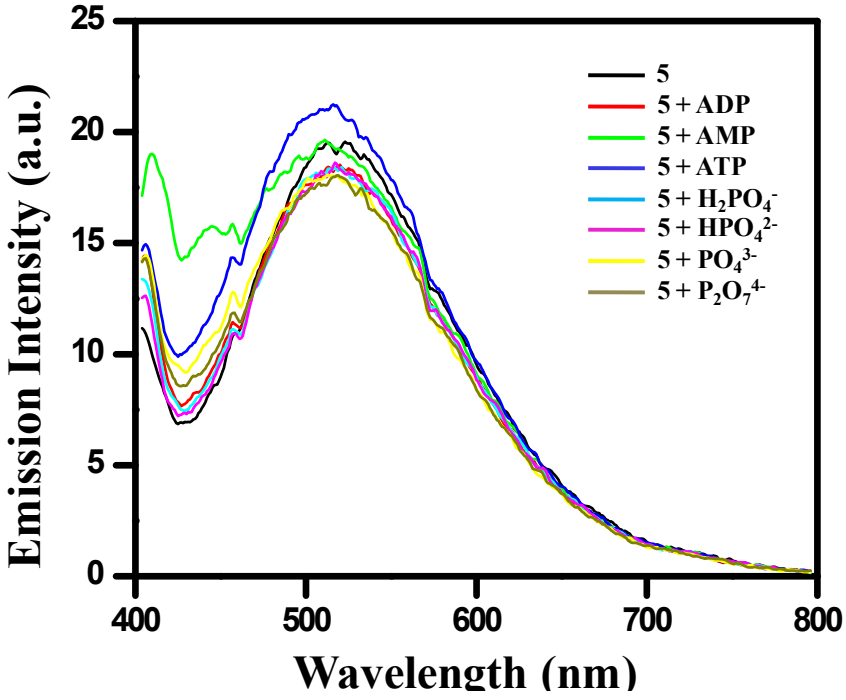

Figure S22. Emission spectra for complex **5** (50 μM) exhibiting negligible change in the emission intensity upon addition of different phosphate ions (5 equiv.). Conditions: solvent; DMSO-H_2O 10% v/v, HEPES, 7.2 pH, λ_{ex} = 330 nm.

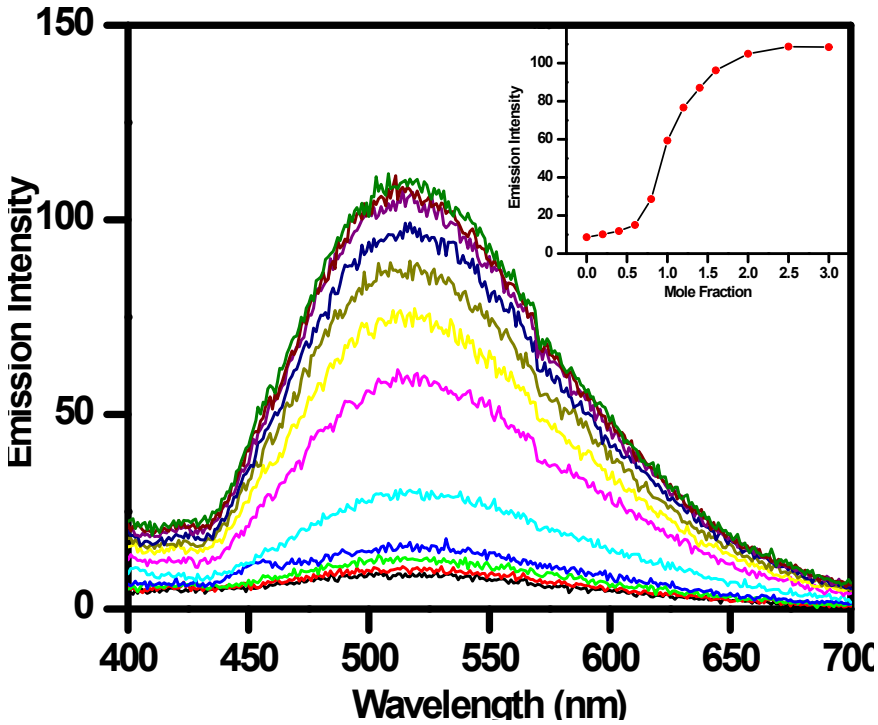

Figure S23. Florescence spectral titration of complex **1** (50 μM) with adenine (0-150 μM) in DMSO-H_2O (10%, v/v). Insets: change in the emission intensity as a function of moles of adenine. Condition: solvent; DMSO-H_2O (10% v/v), HEPES, 7.2 pH, λ_{ex} = 330 nm.

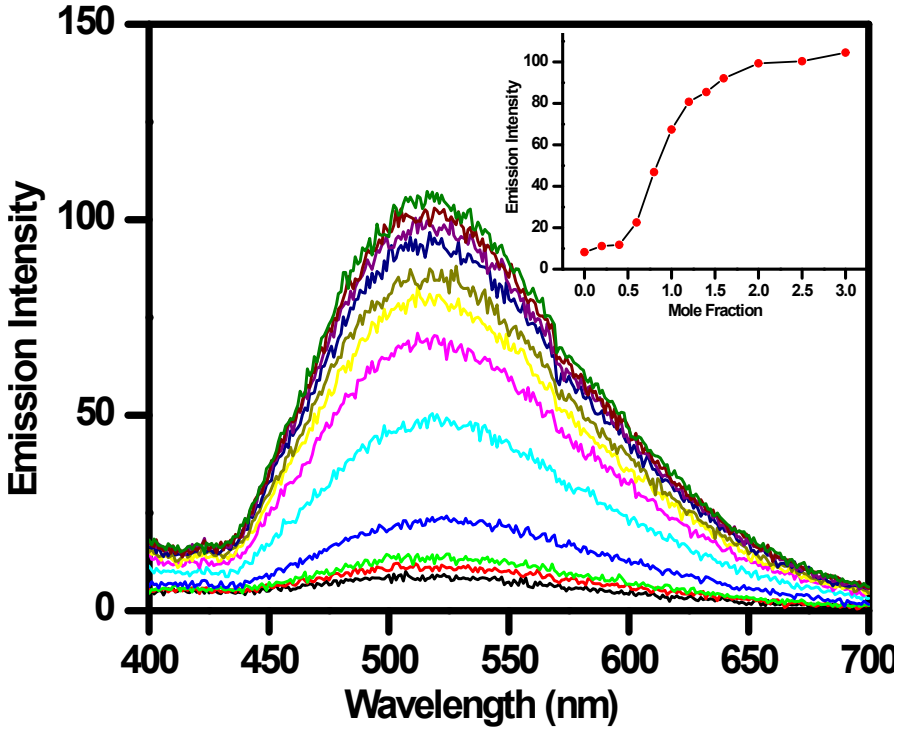

Figure S24. Florescence spectral titration of complex **1** (50 μM) with adenosine (0-150 μM) in DMSO-H_2O (10%, v/v). Insets: change in the emission intensity as a function of moles of adenosine. Condition: solvent; DMSO-H_2O (10% v/v), HEPES, 7.2 pH, λ_{ex} = 330 nm.

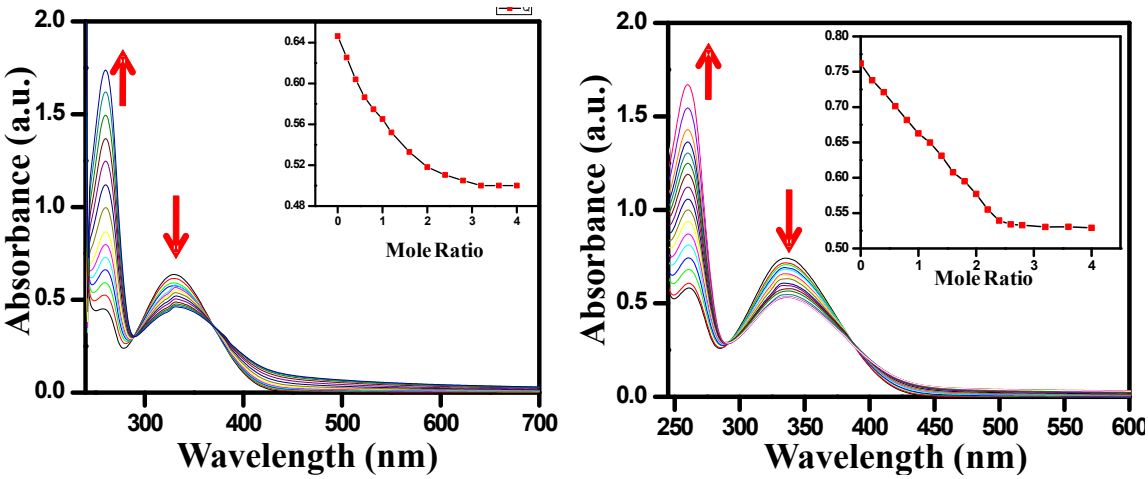

Figure S25. Change in the absorption spectra of complex **1** (50 μM, left) and **2** (50 μM, right) on gradual addition of ATP (0-200 μM). Insets: Plot of absorbance versus moles of ATP added. Conditions; solvent; DMSO-H_2O 10% v/v, HEPES, 7.2 pH.

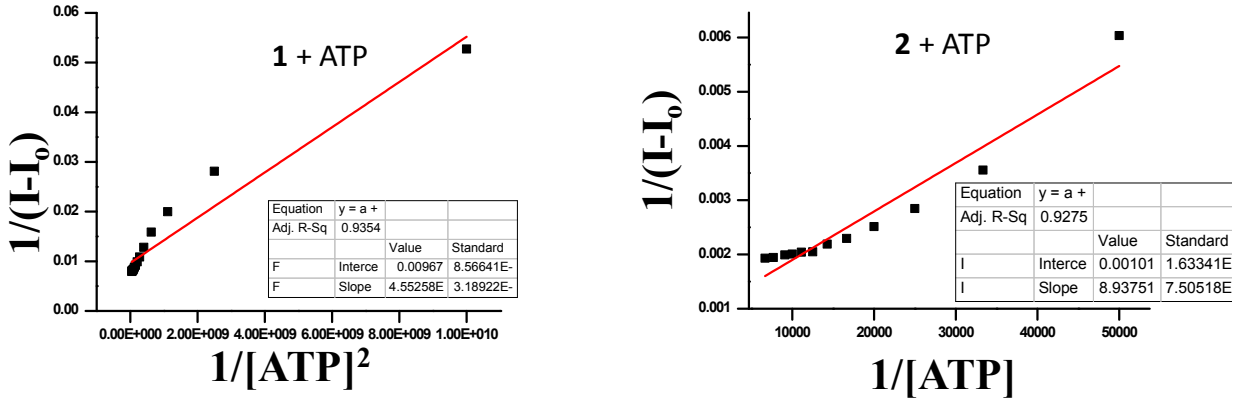

Figure S26. Attempted linear regression fitting for 1:2 binding of complex **1** (left) and 1:1 binding of complex **2** (right) with ATP. Binding Constant (K_b) for 1:2 binding for complex **1**: 21.2 × 10^8 M^{-2}. Binding Constant (K_b) for 1:1 binding for complex **2**: 11.1 x 10^5 M^{-1}.

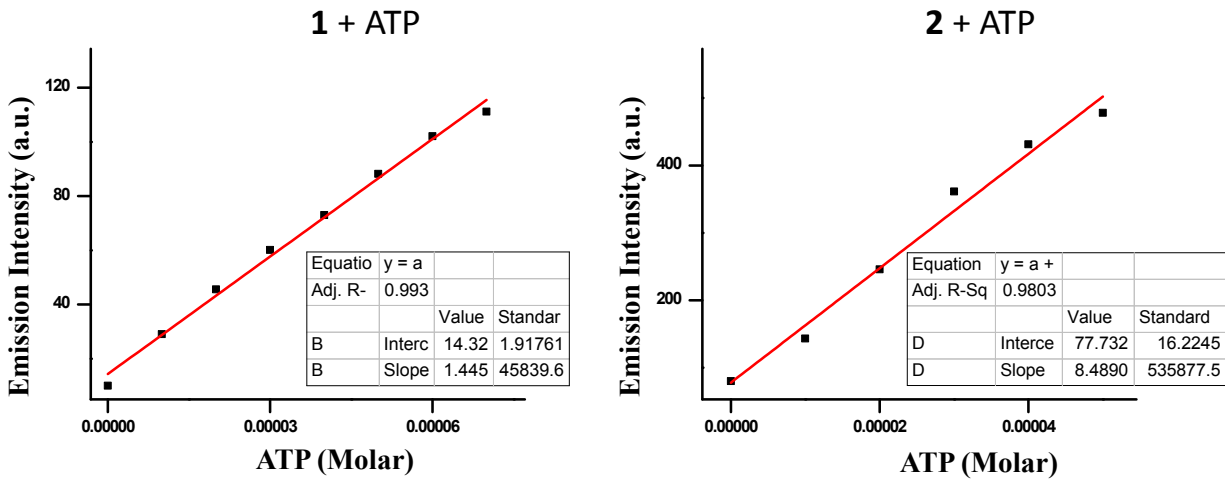

Figure S27. Calculation of Limit of Detection (LOD) for complexes **1** and **2** towards ATP.

The Limit of Detection (LOD) was calculated based on the fluorescence titration. To determine the S/N ratio, the emission intensity of complexes **1** or **2** without ATP was measured 10 times and the standard deviation of blank measurements was determined. The LOD was then calculated with the following equation:

$$LOD = 3 \times SD/S$$

Where SD is the standard deviation of the blank solution measured by 10 times; S is the slope of the calibration curve.

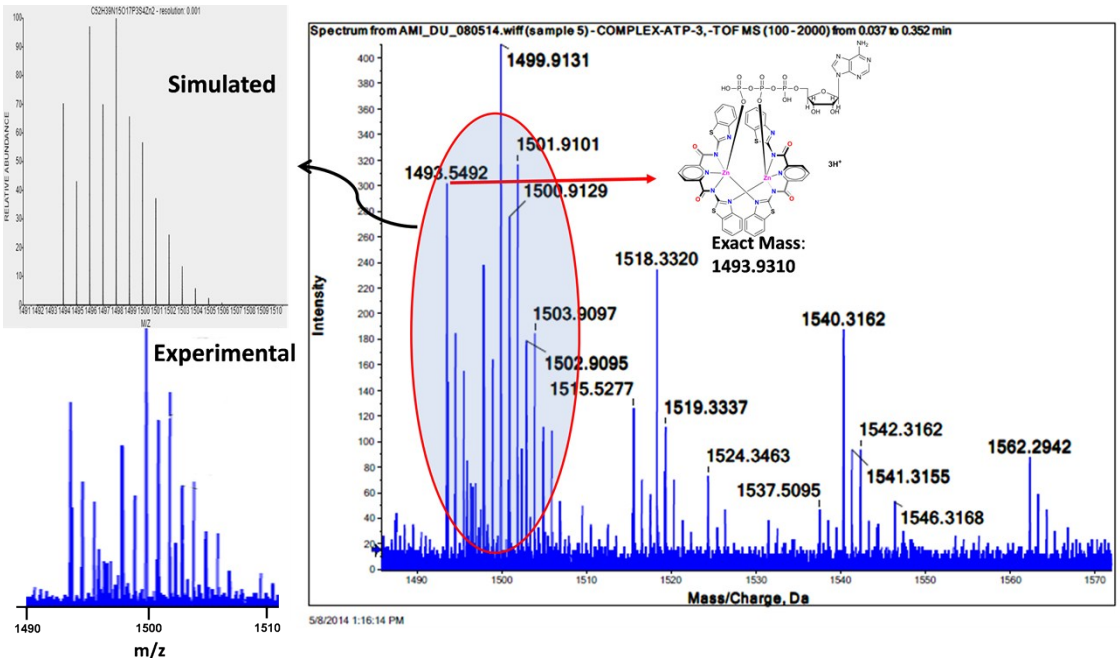

Figure S28. Right: TOF-MS spectrum (recorded in DMSO-H_2O 10% v/v; HEPES, 7.2 pH) showing the peak for adduct of complex **2** with ATP. Left: zoomed in portion showing molecular ion peak (below) with the simulated pattern (above).

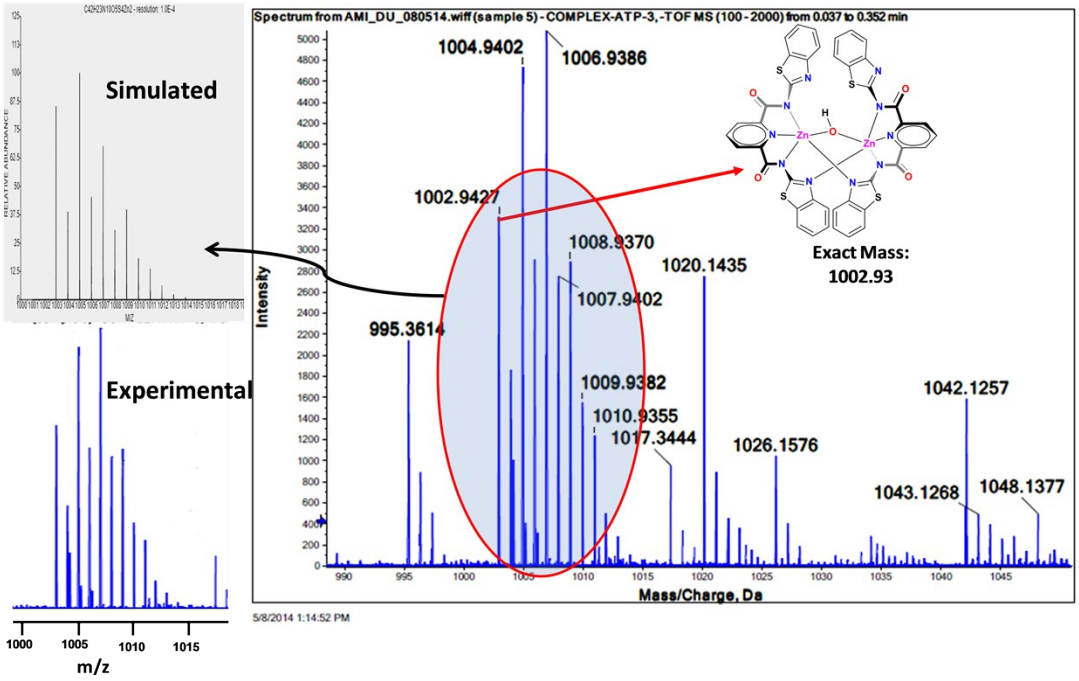

Figure S29. Top: TOF-MS spectrum (recorded in DMSO-H_2O 10% v/v; HEPES, 7.2 pH) showing the presence of peak of the complex **2** in presence of ATP. Left: zoomed in portion showing molecular ion peak (below) with the simulated pattern (above).

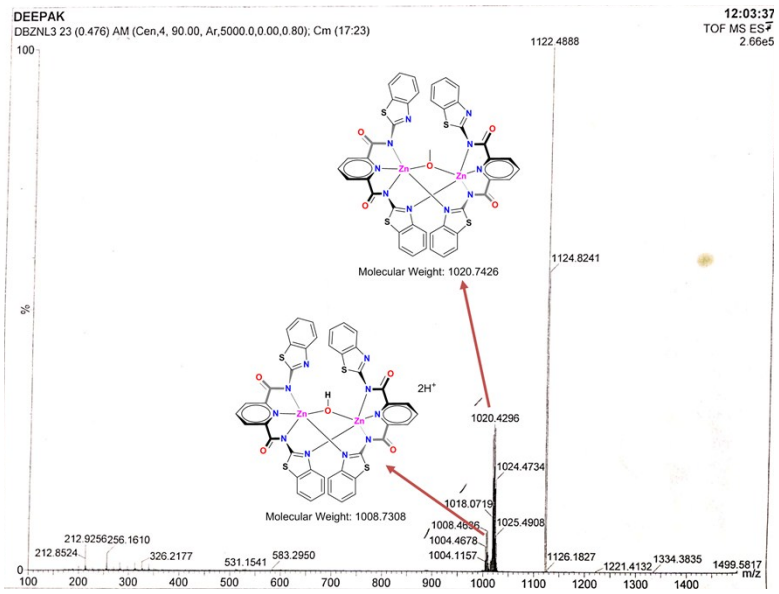

Figure S30. ESI-MS spectrum of complex **2** recorded in methanol.

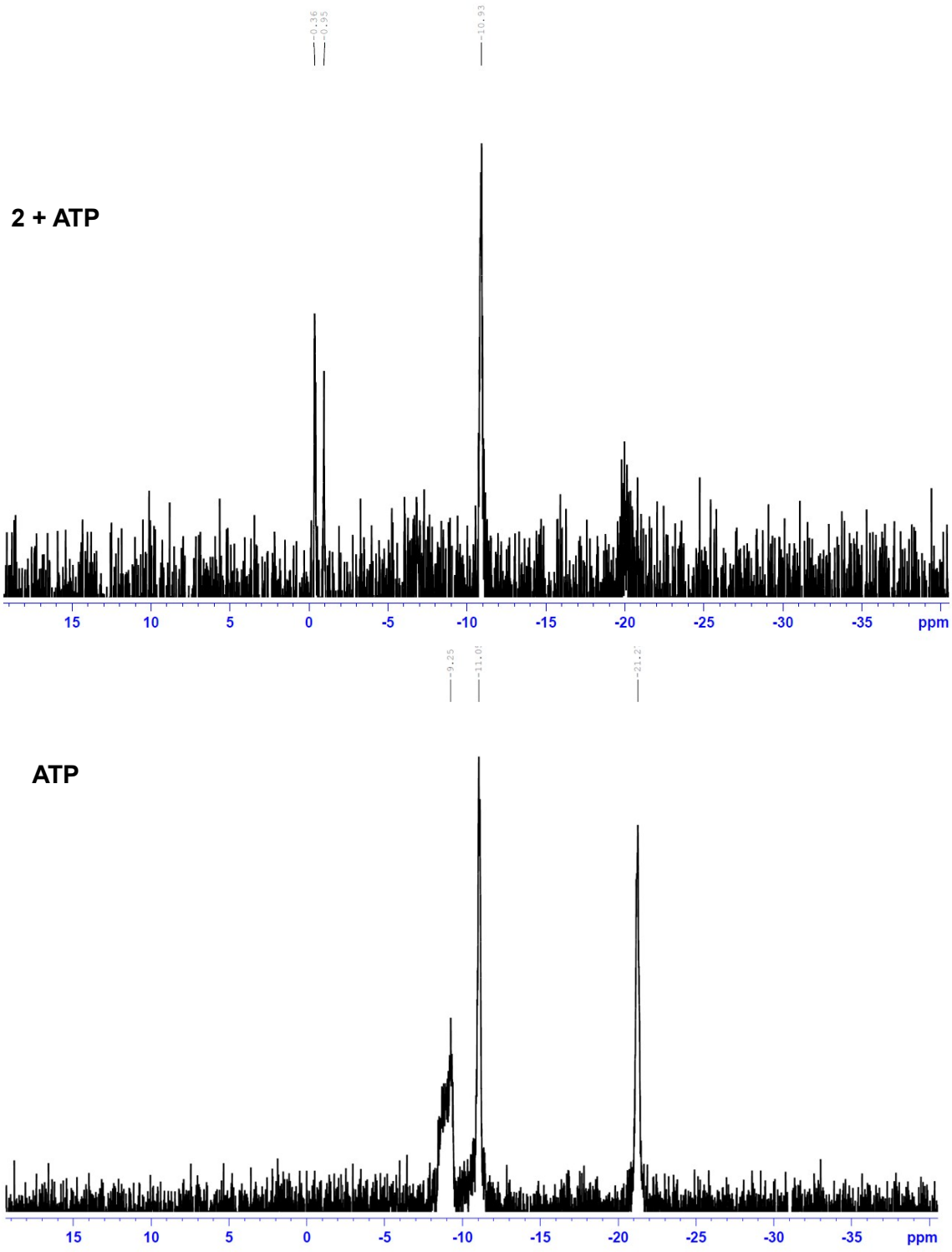

Figure S31. ^{31}P NMR spectrum of ATP alone (bottom) and ATP + complex **2** (top) in DMSO-D_6/D_2O (9:1, v/v).

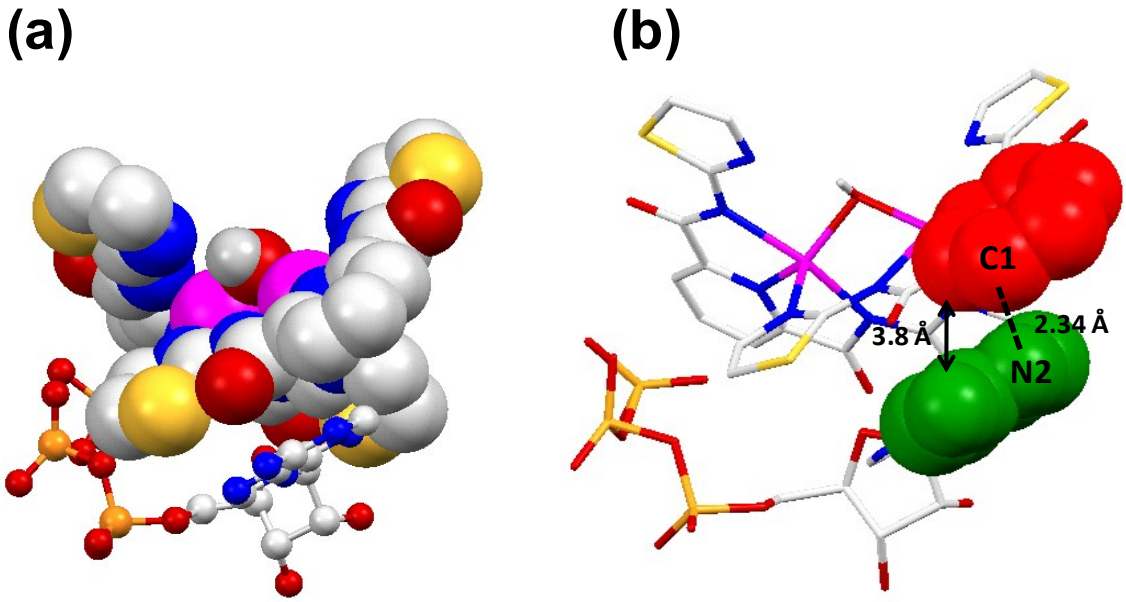

Figure S32. (a) Space-filled docked structure of complex **1** with ATP (shown in ball and stick model). (b) Stick representation of docked structure for complex **1** with ATP (shown in stick representation); pyridine and adenine rings are respectively shown in red and green coloured space-fill representations.

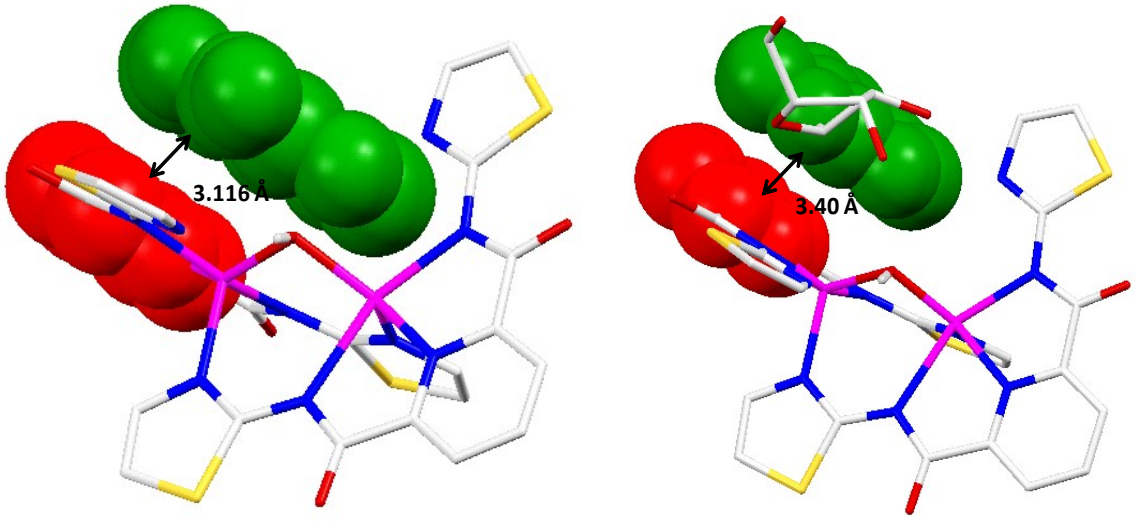

Figure S33. Stick representation of docked structure for complex **1** with adenine (left) and adenosine (right); pyridine and adenine rings are respectively shown in red and green coloured space-fill representations.

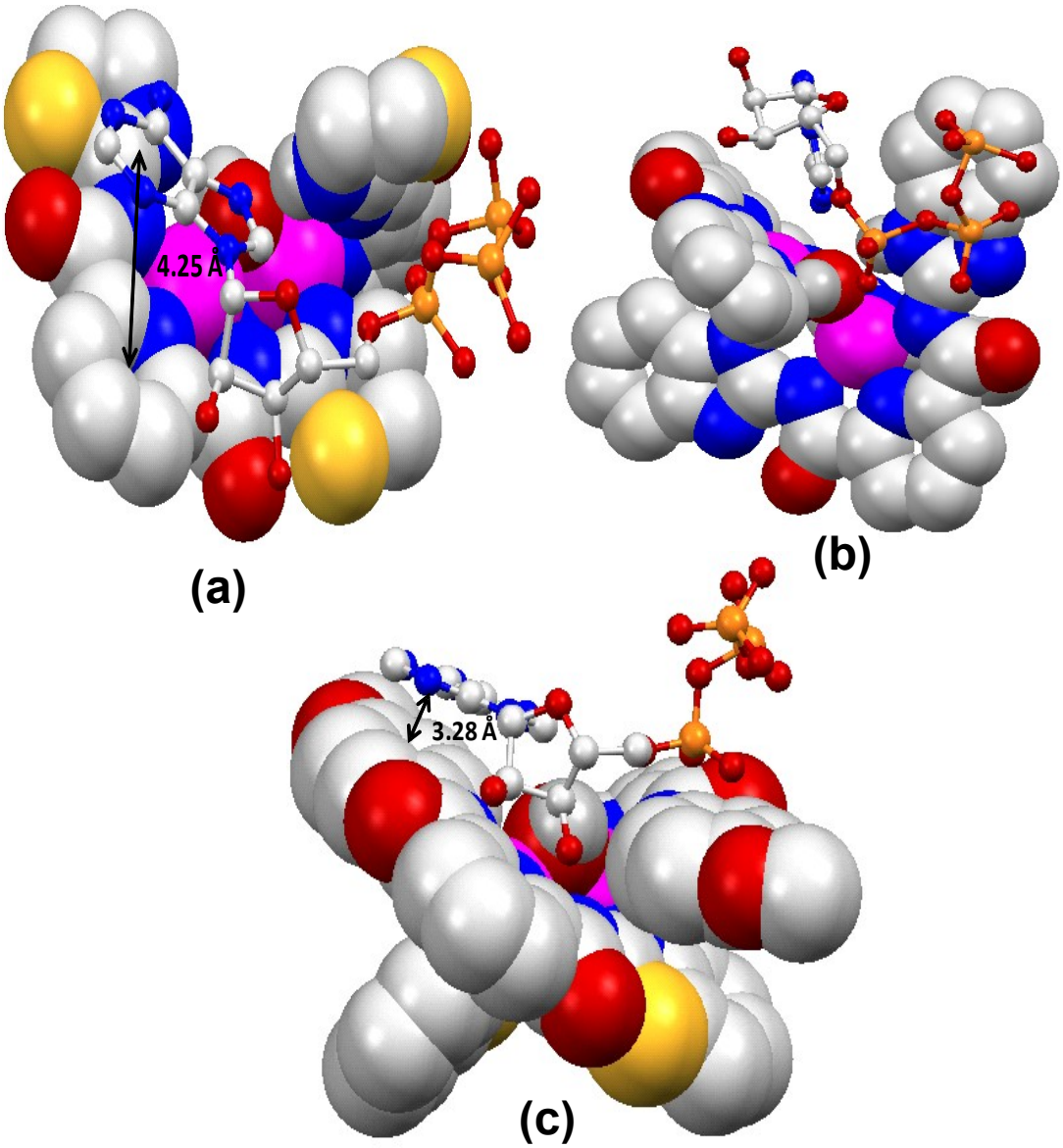

Figure S34. Space-filled docked structures of complex **3** (a), **4** (b) and **5** (c) with ATP (shown in ball and stick model).

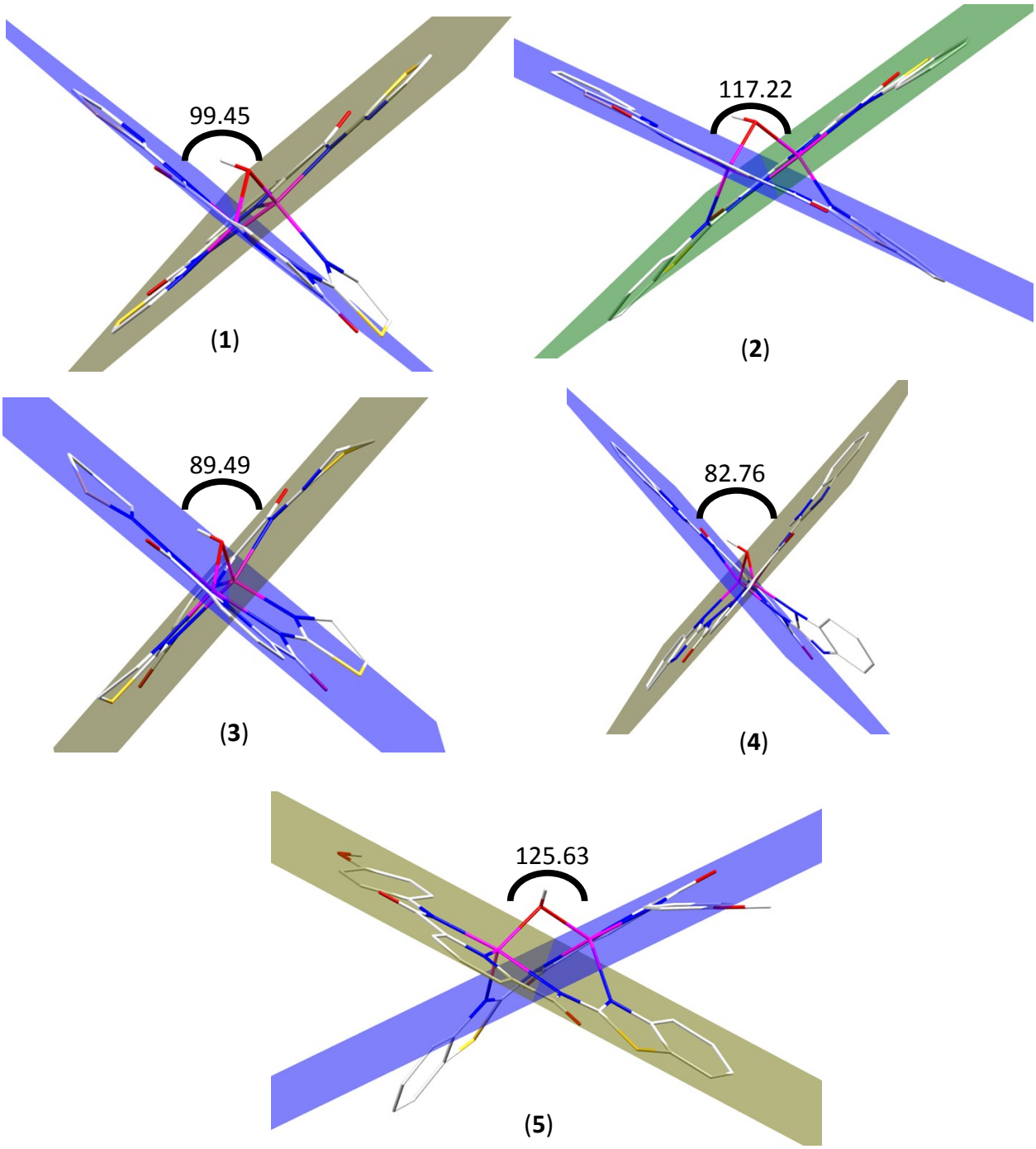

Figure S35. Pictorial representation for the calculation of cone angles in dizinc complexes **1** – **5**.

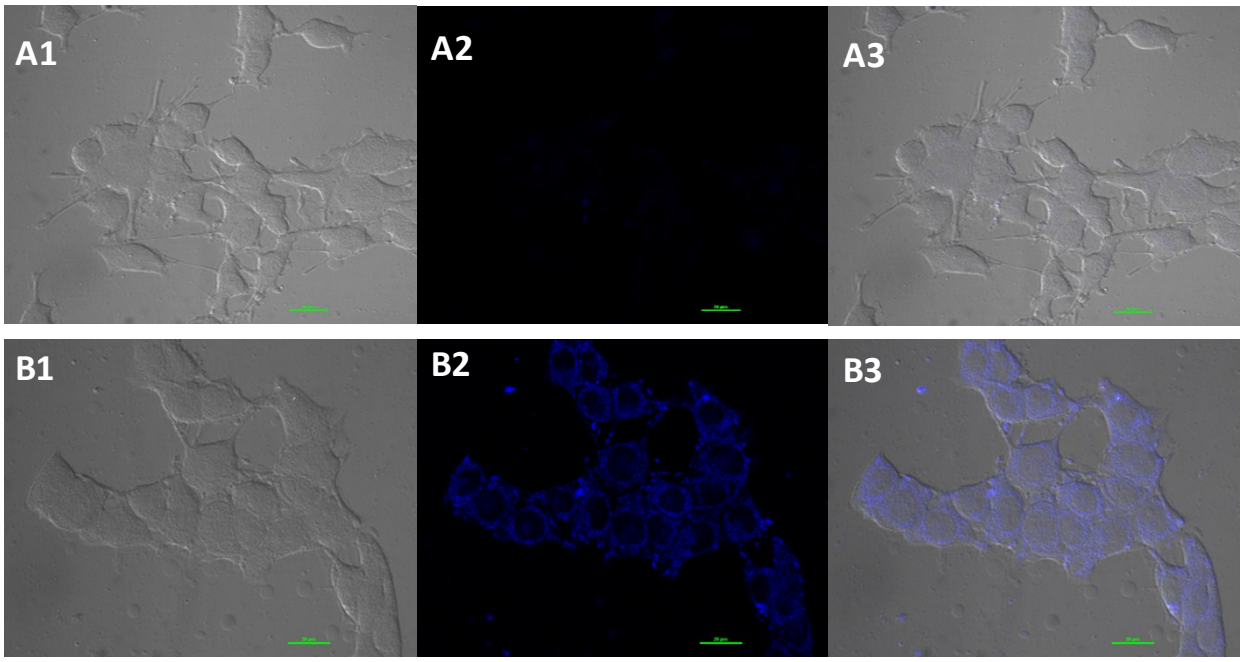

Figure S36. Confocal images of B16 cells; (A1 and B1) Bright field images of cells treated with only solvent used in making the solution of complex **1** (A1) and after treatment with the solution containing complex **1** (B1). (A2 and B2) Fluorescent images of solvent control (A2) exhibiting no emission and cells treated with complex **1** (B2) (λ_{ex} = 400 nm; λ_{em} = 450 nm). (A3 and B3) Overlapped image of A1 with A2 (A3) and B1 with B2 (B3), Scale bar: 20 μm. Conditions: Mitotracker Deep Red (1:500 dilution, 30 min), complex **2** (10 μM, 45 min), pH 7.4.

Table S1. Crystallographic data collection and structure refinement parameters for complexes **1-3**.

	1	**2**	**3**
Chem. Formula	$C_{64}H_{58}N_{24}Na_2O_{14}S_8Zn_4$	$C_{114}H_{116}N_{30}Na_2O_{20}S_8Zn_4$	$C_{26}H_{24}N_{10}O_5S_4Zn_2$
Formula weight	1951.28	2790.30	815.53
Temp (K)	293(2)	170(2)	293(2)
Crystal System	Monoclinic	Monoclinic	Triclinic
Space group	$P2_1/n$	$P2_1/n$	$P\bar{1}$
a [Å]	12.822(5)	16.853(5)	9.782(6)
b [Å]	20.303(5)	21.374(5)	10.109(4)
c [Å]	15.546(5)	17.358(5)	16.854(10)
α [°]	90	90	102.863(4)
β [°]	94.47(5)	90.118(5)	96.007(5)
γ [°]	90	90	106.756(4)
V [Å^3]	4035(2)	6253(3)	1530.30(15)
d [g cm^{-3}]	1.606	1.482	1.770
μ [mm^{-1}]	1.469	0.977	1.898
F(000)	1984	2880	828
R(*int*)	0.0228	0.0193	0.0289
Final *R* indices [I>2σ(I)][a]	R_1 = 0.0313 wR_2 = 0.0751	R_1 = 0.0574 wR_2 = 0.1516	R_1 = 0.0361 wR_2 = 0.0822
R indices (all data)	R_1 = 0.0360 wR_2 = 0.0773	R_1 = 0.0661 wR_2 = 0.1571	R_1 = 0.0439 WR_2 = 0.0870
GOF (F^2)	1.048	1.037	0.834
CCDC No.	1556821	1556822	1556819

[a] $R_1 = \Sigma||F_o|-|F_c||/\ \Sigma|F_o|$; $wR = \{[\Sigma(|F_o|^2|F_c|^2)^2]\}^{1/2}$

Table S2. Crystallographic data collection and structural refinement parameters for complex **5**.

	5
Chem. Formula	$C_{102}H_{100}N_{22}Na_2O_{20}S_4Zn_4$
Formula weight	2389.73
Temp (K)	273(2)
Crystal System	Triclinic
Space group	$P\bar{1}$
a [Å]	12.345(5)
b [Å]	13.843(5)
c [Å]	18.915(5)
α [°]	99.229(5)
β [°]	91.953(5)
γ [°]	115.123(5)
V [Å^3]	2869.8(17)
d [g cm^{-3}]	1.383
μ [mm^{-1}]	0.980
F(000)	1232
R(*int*)	0.0189
Final *R* indices [I>2σ(I)][a]	$R_1 = 0.0483$, w$R_2 = 0.1509$
R indices (all data)	$R_1 = 0.0517$, $wR_2 = 0.1018$
GOF on F^2	0.654
CCDC No.	1556823

[a] $R_1 = \Sigma||F_o|-|F_c||/ \Sigma|F_o|$; $wR = \{[\Sigma(|F_o|^2|F_c|^2)^2]\}^{1/2}$

Table S3. Selected bond lengths (Å) and bond angles (°) for complexes **1 – 4**.

Bond	**1**	**2**	**3**	**4**
Zn1-O5	1.922(2)	1.978(3)	1.943(2)	1.988(8)
Zn1-N9	2.033(2)	2.053(3)	2.019(2)	2.011(9)
Zn1-N2	2.063(2)	2.068(4)	2.060(3)	2.052(9)
Zn1-N1	2.136(2)	2.132(4)	2.249(3)	2.232(9)
Zn1-N3	2.411(2)	2.194(3)	2.176(2)	2.143(9)
Zn1-Zn2	3.139(1)	3.091(1)	3.0533(5)	3.1491(17)
Zn2-O5	1.955(2)	1.945(3)	1.951(2)	1.955(7)
Zn2-N4	2.029(2)	2.043(3)	2.048(3)	2.057(9)
Zn2-N7	2.054(2)	2.068(3)	2.053(3)	2.071(8)
Zn2-N6	2.159(2)	2.140(3)	2.161(3)	2.221(9)
Zn2-N8	2.230(2)	2.270(3)	2.244(2)	2.188(9)
O5-Zn1-N9	112.77(9)	108.50(12)	104.51(10)	108.6(3)
O5-Zn1-N2	136.72(8)	125.50(13)	141.89(10)	141.9(4)
N9-Zn1-N2	108.21(9)	125.96(14)	112.09(10)	109.3(4)
O5-Zn1-N1	107.89(8)	96.22(13)	92.92(9)	99.4(3)
N9-Zn1-N1	99.56(9)	98.52(14)	95.07(9)	94.1(4)
N2-Zn1-N1	77.84(9)	75.45(15)	74.07(10)	74.8(3)
O5-Zn1-N3	90.46(8)	95.83(12)	104.31(10)	97.4(4)
N9-Zn1-N3	94.82(8)	103.24(13)	104.43(9)	104.8(4)
N2-Zn1-N3	72.49(8)	75.41(13)	76.94(10)	76.0(4)
N1-Zn1-N3	149.83(8)	150.26(13)	149.52(10)	149.1(3)
O5-Zn2-N4	107.75(7)	111.59(12)	108.60(10)	103.4(3)
O5-Zn2-N7	138.89(8)	122.66(12)	144.51(10)	145.4(4)
N4-Zn2-N7	113.26(8)	125.20(13)	106.89(10)	110.5(3)
O5-Zn2-N6	95.25(8)	104.75(12)	98.42(11)	94.4(3)
N4-Zn2-N6	99.44(8)	98.16(13)	99.78(11)	98.6(3)
N7-Zn2-N6	75.83(9)	76.26(12)	75.86(12)	74.1(4)
O5-Zn2-N8	100.84(7)	91.03(12)	99.45(10)	103.0(3)
N4-Zn2-N8	99.17(8)	98.73(13)	97.26(10)	102.6(4)
N7-Zn2-N8	75.62(8)	74.39(12)	75.47(10)	76.7(3)
N6-Zn2-N8	150.30(8)	150.66(12)	149.85(11)	148.5(3)

Table S4. Selected bond length (Å) and bond angles (°) for complex **5**.

Bond	**5**	**Bond**	**5**
N4-Zn1	2.053(2)	N6-Zn1-N5	78.98(11)
N5-Zn1	2.119(3)	O7-Zn1-N7	91.46(11)
N6-Zn1	2.054(3)	N4-Zn1-N7	92.45(11)
N7-Zn1	2.423(3)	N6-Zn1-N7	71.71(11)
N1-Zn2	2.115(2)	N5-Zn1-N7	150.61(11)
N2-Zn2	2.051(2)	Zn2-O7-Zn1	109.65(9)
N3-Zn2	2.284(2)	O7-Zn2-N2	124.42(11)
N8-Zn2	2.057(2)	O7-Zn2-N8	116.98(12)
O7-Zn2	1.922(2)	N2-Zn2-N8	116.99(12)
O7-Zn1	1.932(2)	O7-Zn2-N1	110.43(12)
Zn2-Zn1	3.148(1)	N2-Zn2-N1	78.10(12)
O7-Zn1-N4	107.21(12)	N8-Zn2-N1	93.77(12)
O7-Zn1-N6	124.97(12)	O7-Zn2-N3	88.02(11)
N4-Zn1-N6	124.96(12)	N2-Zn2-N3	74.08(11)
O7-Zn1-N5	107.42(11)	N8-Zn2-N3	96.21(12)
N4-Zn1-N5	102.75(11)	N1-Zn2-N3	152.03(11)

Table S5. H-bonding parameters for complexes **1** – **4**.

Complex		A…H–D	A…D	Bond angle (˚)
1	N10…H5 –O5	2.104(2)	2.888(3)	146
2	N5…H7–O5	2.320(5)	3.017(5)	150
3	N10…H5a–O5	2.195(3)	2.834(4)	154
	O5…H5b–N5	2.095(4)	2.847(2)	159
4	N4…H5–O5	2.062(6)	2.914(4)	160
	O5…H10–N10	2.007(2)	2.756(10)	145